

1 **Seasonal cycles of biogeochemical fluxes in the Scotia Sea, Southern Ocean: A stable isotope**  
2 **approach**

3

4 Anna Belcher<sup>1</sup>, Sian F. Henley<sup>2</sup>, Katharine Hendry<sup>1,3</sup>, Marianne Wootton<sup>4</sup>, Lisa Friberg<sup>3</sup>, Ursula  
5 Dallman<sup>2</sup>, Tong Wang<sup>3</sup>, Christopher Coath<sup>3</sup>, Clara Manno<sup>1</sup>

6 <sup>1</sup> British Antarctic Survey, Cambridge, CB3 0ET, UK

7 <sup>2</sup> School of Geosciences, University of Edinburgh, Edinburgh EH9 3FE, UK

8 <sup>3</sup> University of Bristol, Bristol, BS8 1RJ, UK

9 <sup>4</sup> Marine Biological Association, Plymouth, PL1 2PB, UK

10

11 Correspondence to: Anna Belcher ([annbel@bas.ac.uk](mailto:annbel@bas.ac.uk)) and Clara Manno ([clanno@bas.ac.uk](mailto:clanno@bas.ac.uk))

12

13 **Abstract**

14 The biological carbon pump is responsible for much of the decadal variability in the ocean carbon  
15 dioxide (CO<sub>2</sub>) sink, driving the transfer of carbon from the atmosphere to the deep ocean. A  
16 mechanistic understanding of the ecological drivers of particulate organic carbon (POC) flux is key to  
17 both the assessment of the magnitude of the ocean CO<sub>2</sub> sink, as well as for accurate predictions as to  
18 how this will change with changing climate. This is particularly important in the Southern Ocean, a  
19 key region for the uptake of CO<sub>2</sub> and the supply of nutrients to the global thermocline. In this study  
20 we examine sediment trap derived particle fluxes and stable isotope signatures of carbon (C),  
21 nitrogen (N) and biogenic silica (BSi) at a study site in the biologically productive waters of the  
22 northern Scotia Sea in the Southern Ocean. Both deep (2000 m) and shallow (400 m) sediment traps  
23 exhibited two main peaks in POC, particulate nitrogen and BSi flux, one in austral spring and one in  
24 summer, reflecting periods of high surface productivity. Particulate fluxes and isotopic compositions  
25 were similar in both deep and shallow sediment traps, highlighting that most remineralisation  
26 occurred in the upper 400 m of the water column. Differences in the seasonal cycles of isotopic  
27 compositions of C, N and Si provide insights into the degree of coupling of these key nutrients. We  
28 measured increasing isotopic enrichment of POC and BSi in spring, consistent with fractionation  
29 during biological uptake. Since we observed isotopically light particulate material in the traps in  
30 summer, we suggest physically-mediated replenishment of lighter isotopes of key nutrients from  
31 depth, enabling full expression of the isotopic fractionation associated with biological uptake. The  
32 change in the nutrient and remineralisation regimes, indicated by the different isotopic  
33 compositions baselines of the spring and summer productive periods, suggests to a change in the  
34 source region of material reaching the traps, and associated shifts in phytoplankton community  
35 structure. This, combined with the occurrence of advective inputs at certain times of the year,  
36 highlights the need to make synchronous measurements of physical processes to improve our ability  
37 to be able to better track changes in the source regions of sinking particulate material. We also  
38 highlight the need to conduct particle-specific (e.g. faecal pellet, phytoplankton detritus,  
39 zooplankton moults) isotopic analysis to improve the use of this tool in assessing particle

40 composition of ~~the sinking particulate the~~ material and develop our understanding of the drivers of  
41 biogeochemical fluxes.

## 43 1. Introduction

44 The transfer of carbon from the atmosphere to the deep ocean via the biological carbon pump (BCP;  
45 Volk and Hoffert, 1985) is important for the sequestration of carbon, and combined with ocean  
46 circulation is a main driver of decadal variability of the ocean carbon dioxide (CO<sub>2</sub>) sink (DeVries,  
47 2022). Mechanistic understanding of the processes controlling the magnitude and efficiency of the  
48 [biological carbon pump](#)BCP is therefore key to assessment and prediction of the ocean's role as a  
49 CO<sub>2</sub> sink and requires robust characterisation of the composition of the sinking particles transferring  
50 particulate organic carbon (POC) to the deep ocean. [The composition of particles affects the sinking  
51 rate, lability and thus degree of remineralisation as they sink through the water column](#) (e.g. Ploug  
52 et al., 2008; Giering et al., 2020).

53 Sediment traps enable visual assessment of sinking particles, and have been deployed in numerous  
54 locations throughout the world's oceans to both quantify biogeochemical fluxes and characterise the  
55 nature of sinking material (for example data compilation of Atlantic Ocean sediment traps; Torres  
56 Valdés et al., 2014). [Sediment traps can be susceptible to collection biases depending on the depth  
57 of deployment, trap design, hydrodynamic conditions and properties of sinking particles](#) (Buesseler  
58 et al., 2007). [Moored sediment traps can underestimate the actual flux-collect at depths shallower  
59 than ~1500 m by collecting only a portion of the sinking material, though biases vary greatly  
60 between sites](#) (Buesseler et al., 2007). Numerous studies have recorded the dominance of particular  
61 organisms or types of detrital material [in trap material](#), highlighting the importance of ecosystem  
62 community structure on the magnitude and efficiency of the [biological carbon pump](#)BCP. For  
63 example, faecal pellets, diatoms, diatom resting spores and acantharia have been observed as  
64 significant contributors to particle fluxes (González et al., 2009; Belcher et al., 2018, 2017; Manno et  
65 al., 2015; Gleiber et al., 2012; Rembauville et al., 2015; Roca-Marti et al., 2017). Such visual  
66 assessment of trap material is typically very time consuming. Additionally, fragile material, such as  
67 salp faecal pellets (Iversen et al., 2017; Pauli et al., 2021) may break up in the sample manipulation  
68 processes, making them hard to account for visually. Biogeochemical methods such as the use of  
69 stable isotopes may offer additional insight into the drivers of POC fluxes (e.g. Henley et al., 2012).

70 Marine phytoplankton take up aqueous CO<sub>2</sub> ([CO<sub>2(aq)</sub>]) during photosynthesis, converting it to organic  
71 carbon. During this process, the lighter isotope (<sup>12</sup>C) is preferentially assimilated, which enriches the  
72 residual aqueous pool in the heavier isotope (<sup>13</sup>C). The stable isotopic composition of the POC  
73 ( $\delta^{13}\text{C}_{\text{POC}}$ ) of the marine phytoplankton is therefore lower than [that of](#) the carbon source. Over large  
74 scales, the  $\delta^{13}\text{C}$  of marine phytoplankton has been found to be inversely correlated with [CO<sub>2(aq)</sub>] in  
75 surface waters (Rau et al., 1991). However, numerous other factors have been identified as  
76 impacting the  $\delta^{13}\text{C}_{\text{POC}}$  of surface waters and marine plankton. Phytoplankton growth rates, cell  
77 geometry and non-diffusive uptake of carbon via carbon concentration mechanisms have all been  
78 highlighted as impacting the  $\delta^{13}\text{C}_{\text{POC}}$  of marine plankton and thus surface waters (Popp et al., 1999,  
79 1998; Bidigare et al., 1999; Trull and Armand, 2001; Tuerena et al., 2019). This decoupling of the  
80 relationship between  $\delta^{13}\text{C}_{\text{POC}}$  and [CO<sub>2(aq)</sub>] presents [complications-challenges](#) for palaeoceanographic

81 studies, but ~~presents also~~ the possibility of using the  $\delta^{13}\text{C}_{\text{POC}}$  of marine samples to infer information  
82 about community composition.

83 During photosynthetic uptake, the balance between supply and demand of carbon impacts  $\delta^{13}\text{C}_{\text{POC}}$ ,  
84 regulated by the transport into the internal cell and fixation to organic carbon (Popp et al., 1999;  
85 Trull and Armand, 2001). A greater isotopic fractionation occurs in smaller phytoplankton cells,  
86 enabled by the higher cell surface area to volume (SA:V) ratios and increased amount of  $[\text{CO}_{2(aq)}]$   
87 diffusing across the cell membrane relative to the total carbon within the cell (Popp et al., 1998;  
88 Tuerena et al., 2019; Hansman and Sessions, 2016). Thus, a community dominated by large, fast-  
89 growing diatoms is expected to contribute to enriched  $\delta^{13}\text{C}_{\text{POC}}$  values compared to a community  
90 dominated by picoplankton. A study by Henley et al. (2012) in the coastal western Antarctic  
91 Peninsula, attributed a large ( $\sim 10\%$ ) negative isotopic shift in  $\delta^{13}\text{C}_{\text{POC}}$  to a near-complete biomass  
92 dominance of the marine diatom *Proboscia inermis* highlighting the possible impact of shifts in  
93 species composition on stable isotopes. It may therefore be possible to use stable isotopes to gain  
94 information about the community composition of phytoplankton driving, for example, large spring  
95 pulses in POC flux. Additionally, siliceous phytoplankton, such as diatoms, require dissolved silica  
96 (silicic acid, or DSi) to build their cell walls or frustules (amorphous  $\text{SiO}_2 \cdot n\text{H}_2\text{O}$ , referred to here as  
97 biogenic silica, BSi). During uptake of DSi, diatoms fractionate the stable isotopes of silicon ( $^{28}\text{Si}$ ,  $^{29}\text{Si}$ ,  
98  $^{30}\text{Si}$ ) preferentially taking up the lighter isotopes and isotopic fractionation occurs during cell wall  
99 (frustule) formation (De La Rocha et al., 1997). This means that BSi fluxes and ratios of light  $^{28}\text{Si}$  to  
100 heavy  $^{30}\text{Si}$  (expressed as  $\delta^{30}\text{Si}$ ) in sinking particulate organic matter (POM) can be informative about  
101 DSi utilisation by siliceous phytoplankton. The fractionation of Si isotopes during diatom DSi  
102 utilisation is approximately -1.1 ‰, although estimates of this value vary in laboratory and field  
103 studies between -0.5 and -2.5 ‰ (Hendry and Brzezinski, 2014). Whilst some studies have shown  
104 that isotopic fractionation is independent of temperature, DSi and diatom species (e.g., De La Rocha  
105 et al., 1997), one *in vitro* laboratory culture experiment revealed a potential species effect, with  
106 polar species exhibiting more extreme fractionation (-2.09 ‰ for *Chaetoceros* sp. and 0.54 ‰  
107 *Fragilariopsis keruelensis*, (Sutton et al., 2013). The impact of water column dissolution on frustule  
108  $\delta^{30}\text{Si}$  is poorly constrained, with experimental evidence for either a small fractionation of -0.55 ‰  
109 (Demarest et al., 2009) or a negligible impact (Wetzel et al., 2014; Egan et al., 2012; Grasse et al.,  
110 2021)(Wetzel et al., 2014; Egan et al., 2012).

111 Additionally, the stable isotopes of marine nitrogen reveal information about uptake of inorganic  
112 nitrogen sources by phytoplankton (Wada and Hattori, 1978), as well as trophic and food web  
113 processes (Michener and Lajtha, 2008). Nitrogen has two isotopes,  $^{14}\text{N}$ , and  $^{15}\text{N}$ , and the ratio  
114 between these heavy and light isotopes is expressed as  $\delta^{15}\text{N}$ . Different sources of nitrogen can alter  
115 the ~~baseline~~ stable isotopic composition ( ~~$\delta^{15}\text{N}$~~ ) of marine phytoplankton because ammonium  
116 characteristically has a lower value of  $\delta^{15}\text{N}$  than nitrate supplied from depth. As well as this, isotopic  
117 fractionation occurs during transfer through the food web, with a trophic enrichment of typically 2-  
118 4 ‰ between successive trophic levels (Montoya, 2007; Minagawa and Wada, 1984). Excretion and  
119 egestion processes can impact  $\delta^{15}\text{N}$ ; isotopic discrimination during excretion of ammonium by  
120 zooplankton and fish results in ammonium that is  $^{15}\text{N}$ -depleted relative to the substrate catabolised  
121 (Montoya, 2007). Thus, there are several interacting processes impacting the degree of fractionation  
122 and subsequent isotopic ratios in particulate nitrogen (PN) and knowledge of  $\delta^{15}\text{N}$  ratios may  
123 provide insight into biogeochemical processes and the composition of the sinking flux.

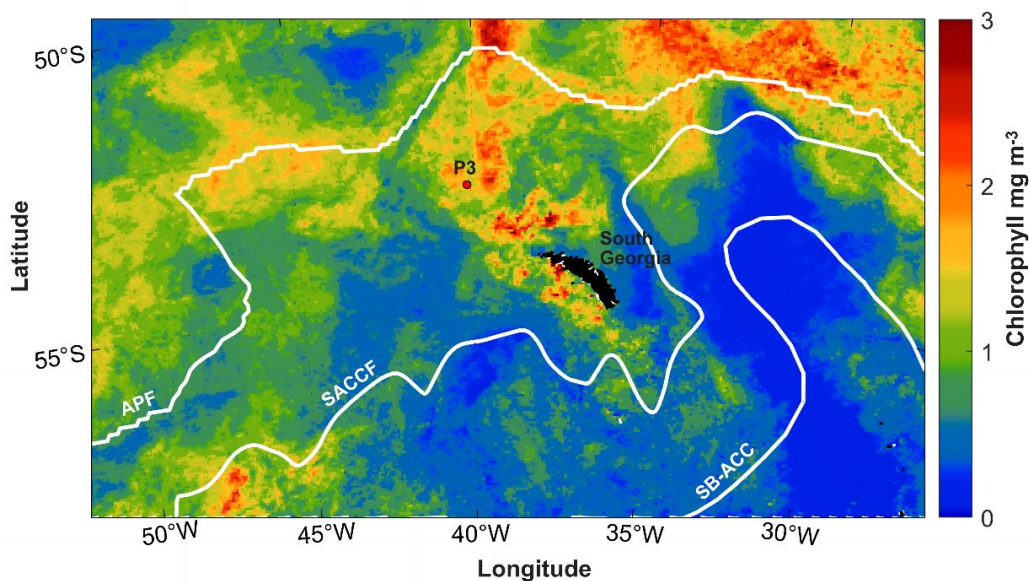
124 In this study we examine the seasonal cycle, of the magnitude and composition of vertical  
125 biogeochemical fluxes of particulate material collected by two sediment traps deployed for almost  
126 one year-year on a deep ocean mooring located in the northern Scotia Sea in the ~~(Atlantic sector of~~  
127 ~~the Southern Ocean)~~. The Scotia Sea, particularly the region downstream of South Georgia is a hot  
128 spot for biological productivity, supported by higher iron availability (Korb et al., 2008; Matano et al.,  
129 2020). Diatoms dominate the phytoplankton assemblage, particularly in the summer months, with  
130 smaller contributions of dinoflagellates (Korb et al., 2012). The large, consistent phytoplankton  
131 blooms occurring in this region support high fluxes of POC to the deep ocean, with two peaks in POC  
132 flux occurring during the seasonal cycle: ~~{~~first peak in austral spring, and second in late summer or  
133 early autumn~~}~~ (Manno et al., 2015). Faecal pellets (up to 91% in late spring and early summer,  
134 seasonally ~~{~~(Manno et al., 2015)~~}~~, krill exuviae (up to 47% in summer, seasonally ~~{~~(Manno et al.,  
135 2020)~~}~~) and diatoms, particularly resting spores (annual contribution of 42%, annually ~~{~~(Rembauville  
136 et al., 2016)~~}~~) have been shown to make ~~a~~ large contributions to the POC fluxes in our study region.  
137 Here we use  $\delta^{13}\text{C}_{\text{POC}}$ ,  $\delta^{15}\text{N}_{\text{PN}}$  and  $\delta^{30}\text{Si}_{\text{BSi}}$  alongside calculated fluxes of POC, PN and BSi as tools to  
138 reveal information on the composition of about sinking particulate organic matter and the processes  
139 influencing its production and subsequent flux to depth. More in-depth understanding of the  
140 composition, and thus the drivers of POC flux in this important region are key to improving estimates  
141 of the current and future strength of the biological carbon pump~~BCP~~ and the ocean's role as a  $\text{CO}_2$   
142 sink.

143

## 144 2. Methods

### 145 2.1. Study Area

146 This study was conducted in the open ocean environment of the northern Scotia Sea in the Southern  
147 Ocean at a long-term observatory station, P3 (Figure 1), where an oceanographic mooring is located.  
148 The mooring is part of the Scotia Sea Open Ocean Observatory (SCOOBIES:  
149 <https://www.bas.ac.uk/project/scoobies/>), a programme designed to investigate the biological and  
150 biogeochemical influence of the large and persistent phytoplankton bloom to the northwest of  
151 South Georgia.



152

153 **Figure 1: Location of P3 mooring site to the northwest of South Georgia. White lines indicate**  
154 **frontal positions of the Antarctic Polar Front (APF) (Moore et al., 1999), Southern ~~Atlantic~~Antarctic**  
155 **Circumpolar Current Front (SACCF) (Thorpe et al., 2002) and the Southern Boundary of the**  
156 **Antarctic Circumpolar Current (SB-ACC) (Orsi et al., 1995). Mean chlorophyll concentration ( $\text{mg m}^{-3}$ )**  
157 **is shown for December 2018 from 8-day satellite chlorophyll data from the Ocean Colour CCI**  
158 **(version 5.0) (Sathyendranath et al., 2021, 2019).**

159

## 160 2.2. Sediment trap deployment

161 Two sediment traps were deployed on the mooring array to collect sinking particles for analysis of  
162 carbon, nitrogen and biogenic silica fluxes and analysis of  $\delta^{13}\text{C}_{\text{POC}}$ ,  $\delta^{15}\text{N}_{\text{PN}}$  and  $\delta^{30}\text{Si}_{\text{BSi}}$ . The mooring  
163 was deployed from 25<sup>th</sup> January 2018, during research cruise JR17002 aboard the *RRS James Clark*  
164 *Ross*, to 1<sup>st</sup> January 2019, recovered during research cruise DY098 aboard the *RRS Discovery*. The  
165 mooring was located at  $-52.8036^\circ\text{S}$ ,  $-40.1593^\circ\text{W}$ , to the northwest of South Georgia island in the  
166 Scotia Sea at a water depth of 3748 m. Sediment traps (McLane PARFLUX, 0.5 m<sup>2</sup> surface collecting  
167 area; McLane labs, Falmouth, MA, USA) were deployed at 400 and 2000 m (referred herein as  
168 shallow and deep respectively) and were each equipped with 21 sample bottles. A baffle at the top  
169 of the trap prevents large organisms from entering and each [sample](#) bottle contained a formosaline  
170 solution (filtered seawater containing 2% v/v formalin, mixed with sodium tetraborate (BORAX;  
171 0.025% w/v), and 0.5% w/v sodium chloride) to prevent mixing with the overlying water column  
172 and stop biological degradation. Previous studies have reported the effects of formalin on  $\delta^{13}\text{C}_{\text{POC}}$   
173 and  $\delta^{15}\text{N}_{\text{PN}}$  to be small ( $\pm 1\text{‰}$  and  $\pm 1.5\text{‰}$  respectively, ~~{Mincks et al., 2008 and references therein}~~  
174 ~~within~~). ~~This which equates to 13% and 165.8% of the maximum range measured in our study}~~  
175 ~~(Mincks et al., 2008 and refs. within)~~, which ~~is~~ are small compared to the isotopic shifts we observed.  
176 Yet we stress that all  ~~$\delta^{13}\text{C}_{\text{POC}}$  and  $\delta^{15}\text{N}_{\text{PN}}$  given~~ values ~~given here~~ are associated with this uncertainty.  
177 The sediment trap sample carousel was programmed to rotate every 7-31 days depending on the  
178 season; shorter periods to coincide with austral summer and longer periods during austral winter  
179 (Table S1). ~~TM~~ Seaguard current meters were deployed ~50 m above ~~the shallow sediment trap and~~  
180 ~~50 m below the /below the shallow/deep sediment traps respectively~~, set at a measurement interval  
181 of 2 hours.

## 182 2.3. Trap sample processing

183 Each sample [bottle](#) from the sediment trap was processed on return to the laboratory. The  
184 supernatant was carefully removed using a syringe and swimmers (zooplankton that are believed to  
185 have entered the trap actively whilst alive) were removed. Swimmers were removed by hand under  
186 a dissecting microscope and were not included in flux calculations. ~~The material from E~~each  
187 [sediment trap](#) sample [bottle](#) was split into a number of smaller aliquots for subsequent analysis  
188 using a McLane rotary splitter.

189

### 190 2.3.1. Organic carbon and nitrogen

191 For each sediment trap ~~sample bottle~~ (from both deep and shallow traps), two or three splits were  
192 ~~taken and each~~ analysed for POC and PN ~~mass and  $\delta^{13}\text{C}_{\text{POC}}$  and  $\delta^{15}\text{N}_{\text{PN}}$~~ . Once split, the material was  
193 filtered onto pre-combusted (450 °C, 16h) 25 mm glass fibre filters (GF/F; ~~nominal pore size 0.7  $\mu\text{m}$~~ )



194 and rinsed with milli-Q water. Samples were air dried, ~~before fum~~ed for 24 h with 37% HCl in a  
195 desiccator, before finally oven-drying at 50 °C for 24 h. Filters and filter blanks were placed in sterile  
196 tin capsules and POC and PN measured on a CE Instruments NA2500 Elemental analyser, calibrated  
197 using an acetanilide calibration standard with a known %C and %N of 71.09% and 10.36%  
198 respectively. Standards were interspersed regularly between samples to measure and correct for  
199 drift. Analytical precision was better than 1.0% for POC and 1.1% for PN. The POC flux ( $F$ ,  $mg\ C\ m^{-2}$   
200  $d^{-1}$ ) for each sample was calculated using the following equation:

$$201 \quad F(mg\ C\ m^{-2}\ d^{-1}) = m/(A \times d) \quad (1)$$

202 Here  $m$  is the mass of POC in the sample bottle (mg),  $d$  is the number of days that the sample bottle  
203 was open (7–31 days) and  $A$  is the surface area of the sediment trap opening (0.5 m<sup>2</sup>). The same  
204 calculation was carried out for PN.

205 ~~An additional two splits were taken from each sample bottle for analysis of both~~  $\delta^{13}C_{POC}$  and  $\delta^{15}N_{PN}$ .  
206 ~~These samples were processed as above for POC and PN but~~ were analysed on a Thermo Finnigan  
207 Delta-Plus Advantage isotope ratio mass spectrometer that was in line with the elemental analyser.  
208 All  $\delta^{13}C_{POC}$  and  $\delta^{15}N_{PN}$  data are presented in the as delta per mille (‰) notation enrichment relative to  
209 the appropriate international a-standard, according to equation 2.

$$210 \quad \delta X(\text{‰}) = 10^3(R_{sample}/R_{standard} - 1) \quad (2)$$

211 ~~where~~  $R$  denotes the  $^{13}C/^{12}C$  ratio for carbon or the  $^{15}N/^{14}N$  ratio for nitrogen.  $R_{sample}$  refers to the  
212 relevant ratio in the sample.  $R_{standard}$  refers to the ratios in the international standards Vienna Pee  
213 Dee belemnite (V-PDB used as reference material for  $\delta^{13}C$  and atmospheric nitrogen (AIR) for  $\delta^{15}N$   
214 which is Vienna-Pee-Dee belemnite (V-PDB) and atmospheric nitrogen (AIR) respectively, both of  
215 which ~~we~~ are calibrated against the PACS-2 marine sediment reference material international  
216 standard. Multiple repeats of analytical standards gives a reproducibility of 0.2‰ for C and N, which  
217 is significantly smaller than the uncertainty associated possible effects with of organic carbon in the  
218 formalin preservation (±1‰ and ±1.5‰ for C and N respectively) (Mincks et al., 2008 and  
219 references therein refs. within).

220

### 221 2.3.2. Biogenic silica

222 Two splits were taken ~~for~~ from each sediment trap sample bottle ~~sample~~ (from both deep and shallow  
223 sediment traps) for analysis of biogenic silica and silicon isotopes. Split material was filtered onto 25  
224 mm, 0.4 µm, polycarbonate filters and rinsed with Milli-Q water before drying at 50 °C for 24h.  
225 Material on the filters was solubilised via an alkaline extraction method (Hatton et al., 2019) carried  
226 out at the Bristol Isotope Group (BIG) laboratory. Sample material was digested in Teflon tubes with  
227 0.2M NaOH at 100 °C for 40 minutes. This was followed by neutralisation with 6M HCl. Biogenic silica  
228 (SiO<sub>2</sub>, termed BSi) concentrations were measured chlorometrically by molybdate blue  
229 spectrophotometry (Heteropoly Blue Method) (Strickland and Parsons, 1972) using a Hach DR3900  
230 spectrophotometer set at a wavelength of 815 nm. Supernatants were stored for 7-11 months  
231 before column chemistry for isotope analysis. Fluxes of biogenic silica were calculated as for POC  
232 using equation 1.

233 For Si isotope analysis, supernatants and reference [materials-standards](#) were purified by passing  
234 through ~~pre-cleaned~~ cation exchange columns (Bio-Rad AG50W-X12, 200-400 mesh resin) ~~pre-~~  
235 ~~cleaned with HCl~~ following ~~(Georg et al., (2006) using HCl as eluent.~~ Samples were acidified to a pH  
236 of 1-2 to ensure that all the silicon remained in solution. Samples were loaded onto columns and  
237 eluted with Milli-Q water to produce a 2.5 ppm solution, and concentrations ~~were~~ checked to  
238 confirm quantitative yields. Si isotopic composition was analysed within 24 hours of column  
239 chemistry. Stable Si isotopic compositions were measured at the BIG laboratory on a Finnigan  
240 Neptune Plus High-Resolution MC-ICP-MS (Thermo Fisher Scientific). The Si solutions were spiked  
241 with magnesium spike (Inorganic Ventures MSMG-10 ppm), hydrochloric acid (1M HCl in-house  
242 distilled) and sulphuric acid (0.1M H<sub>2</sub>SO<sub>4</sub>, ROMIL-UpA™ Ultra Purity Sulphuric Acid), and transferred  
243 from the autosampler via a PFA Savillex C-Flow nebulizer (35 µl min<sup>-1</sup>) connected to an Apex IR  
244 Desolvating Nebulizer (Ward et al., 2022), and measured on the low-mass side to resolve any  
245 isobaric interferences (e.g., <sup>14</sup>N<sup>16</sup>O<sup>+</sup>). All standards and samples were blank-~~corrected~~ offline. The  
246 intensity of <sup>28</sup>Si in the 0.1M HCl blank was <1% of the sample intensity in all sample runs.  
247 Furthermore, we also measured Mg isotopes (<sup>24</sup>Mg, <sup>25</sup>Mg and <sup>26</sup>Mg) as an internal isotopic reference  
248 to correct for any mass-dependent fractionation (White et al., 2000). Measurements that resulted in  
249 large corrections (>0.3‰ on δ<sup>30</sup>Si) underwent repeat analysis. Instrumental mass bias was further  
250 accounted for using a standard-sample bracketing method using a 2 ppm reference standard (NBS or  
251 RM8546) solution. Two ~~splitsamples~~ were analysed for each sediment trap bottle ~~(pseudo-replicates~~  
252 ~~as the sediment trap material was heterogeneous)~~, as well as standards and sample blanks.  
253 Solutions ~~obtained from each split~~ were measured in replicate (n = 2-3) alongside continuous  
254 measurement of reference ~~standards-materials~~ Diatomite and LMG-08 to ensure reproducibility and  
255 to monitor data quality. Measurements of Diatomite and LMG-08 yielded δ<sup>30</sup>Si of +1.23‰ (SD ±  
256 0.03, n=18) and -3.40‰ (SD ± 0.05, n=5) respectively, which agreed with published values (Reynolds  
257 et al., 2007; Hendry and Robinson, 2012; Grasse et al., 2017). Typical reproducibility between the  
258 ~~sediment trap sample splits (coming from the same sediment trap bottle)-ample pseudo-replicates~~  
259 ~~was 0.034‰ (1 x SD). A lithogenic correction (e.g. Closset et al., 2015) was not carried out on these~~  
260 ~~samples. However, even an extreme scenario of variable lithogenic contamination of 1-5 % of~~  
261 ~~isotopically light marine clays (with δ<sup>30</sup>Si of -2.3 ‰; Opfergelt and Delmelle, 2012) would only result~~  
262 ~~in a potential systematic offset of 0.12 ‰, which is an order of magnitude smaller~~less~~ than the~~  
263 ~~observed seasonal signal.~~

#### 264 *Chlorophyll and phytoplankton community composition*

265 Surface chlorophyll concentrations were obtained from [satellite-derived 8-day](#) Ocean Colour CCI  
266 (version 5.0) (Sathyendranath et al., 2021, 2019). ~~We present the monthly mean of these 8-day data~~  
267 ~~for December at our study site (Figure 1), We present the mean of 8-day concentrations for~~  
268 ~~December 2018 as as~~ well as ~~the seasonal cycle of 8-day averaged chlorophyll concentrations the 8-~~  
269 ~~day chlorophyll concentration data from September 2017 to December 2018 (Figure 2)~~ averaged  
270 over a 1 x 1° bounding box around our study site (-41 °~~WE~~, -40 °~~WE~~, -53 °~~SN~~, -52 °~~SN~~).

271 ~~Light microscopy was used to assess Pp~~ phytoplankton and microzooplankton community composition  
272 of a small selection of samples from the two main productive periods, ~~were assessed via light~~  
273 ~~microscope~~. A biological method of sample preparation and analysis was chosen, comparable with  
274 Rembauville et al. (2015), to determine the quantity of empty and full cells. Following subsampling  
275 using the rotary splitter, samples for morphological taxonomic analysis were diluted to a

276 standardised 25 ml. Samples were gently [inverted using the Paul Schatz principle \(figures of eight\)](#)  
277 [for one minute to](#) homogenise [them](#), and 2 ml [was](#) withdrawn using a modified pipette with  
278 widened opening. Several common diatoms in Antarctic waters are long and slim; in particular,  
279 *Thalassiothrix antarctica* has been recorded with an apical axis up to 5mm. To ensure such  
280 specimens remain intact and are not excluded from the pipetting process, a wide bore opening is  
281 necessary. The 2 ml subsamples were used to fill a 1 ml Sedgwick Rafter counting chamber.  
282 Chambers were viewed using a compound light microscope (Nikon Eclipse 80i) with differential  
283 interference contrast at x200 magnification. For the larger, easily identifiable cells, the whole  
284 chamber was observed; for smaller cells a proportion of the chamber was examined depending upon  
285 cell abundance (at least 500 cells were counted). Only complete cells were enumerated to avoid  
286 over counting of fragmented specimens. Cells were determined as “full” or alive at time of collection  
287 if they possessed chloroplasts/plastids, pigment, a nucleus or, in the case of *Pronoctiluca*, a distinct  
288 accumulation body; cells lacking these internal features were deemed as “empty”, or dead at time of  
289 collection. Specimens were identified according to Hasle and Syvertsen (1997); Medlin and Priddle  
290 (1990); Priddle and Fryxell (1985) and Scott and Marchan (2005).

291 Cell bio-volume and surface area estimates were calculated using geometrics and [the appropriate](#)  
292 [shape-](#)related equations for phytoplankton genera proposed by Hillebrand et al. (1999). Metrics  
293 used in the calculations were based on the average size of ten randomly selected specimens  
294 belonging to a species/taxonomic group within the samples.

295

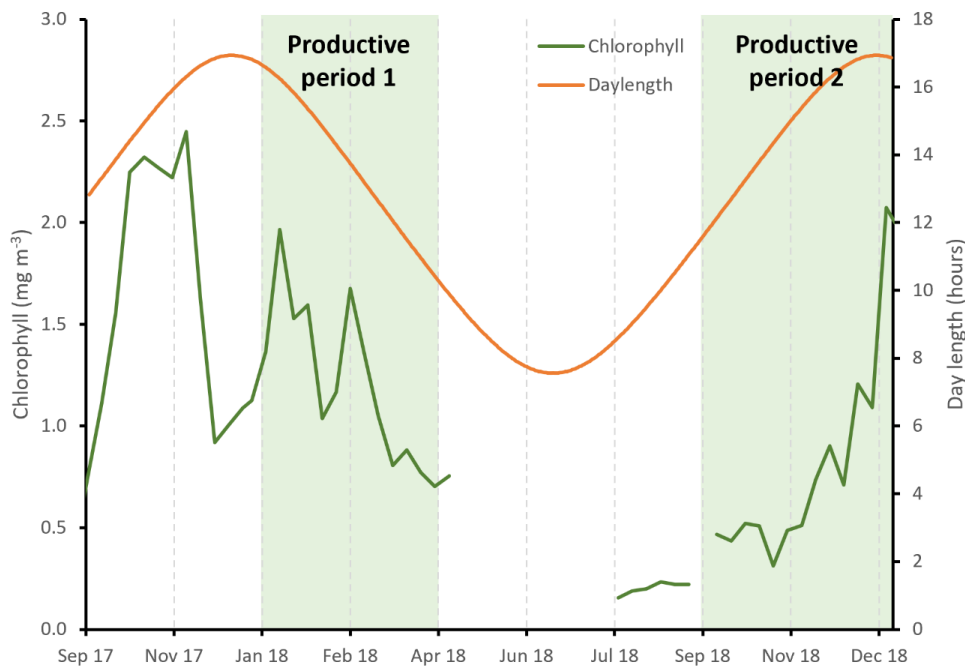
### 296 3. Results

#### 297 3.1. Environmental conditions

298 Mean current velocities were 0.11 ( $\pm 0.06$ ) and 0.06 ( $\pm 0.03$ ) m s<sup>-1</sup> for shallow and deep current  
299 meters respectively (Supplementary Figure S1). Maximum current speeds recorded reached 0.43  
300 and 0.18 m s<sup>-1</sup> for shallow and deep meters respectively. The periods with currents substantially  
301 elevated above the mean were June for both traps, and additionally in late August/September for  
302 the shallow trap, both for periods of ~5-10 days. Both are periods of low fluxes during austral winter  
303 and are not the main subject of the study here, though it is likely that particle collection was biased  
304 at these times (Buesseler et al., 2007).

305 Satellite-derived estimates of surface chlorophyll show high concentrations during austral summer  
306 (January to March) peaking at 2.3 mg m<sup>-3</sup>, as well as during spring (November-December), peaking at  
307 2.1 mg m<sup>-3</sup> (Figure 2, Figure S2). Data coverage is limited in the winter due to cloud cover, but  
308 concentrations appear to be [<0.41](#) mg m<sup>-3</sup>. We define here two productive periods (when  
309 chlorophyll concentrations were >0.4 mg m<sup>-3</sup>), which we refer to throughout the manuscript,  
310 productive period 1: January to April 2018, and productive period 2: September to December 2018.  
311 [We note that our sediment trap data begins on the 25<sup>th</sup> January so we do not capture the start of](#)  
312 [period 1.](#)





313

314 **Figure 2: Seasonal cycle of satellite derived surface chlorophyll concentration (green line, 8-day**  
 315 **data from the Ocean Colour CCI (version 5.0) (Sathyendranath et al., 2021, 2019)). Daylength at -53**  
 316 **°S is shown by the orange line. The two productive periods are highlighted by the shaded green**  
 317 **region.**

318

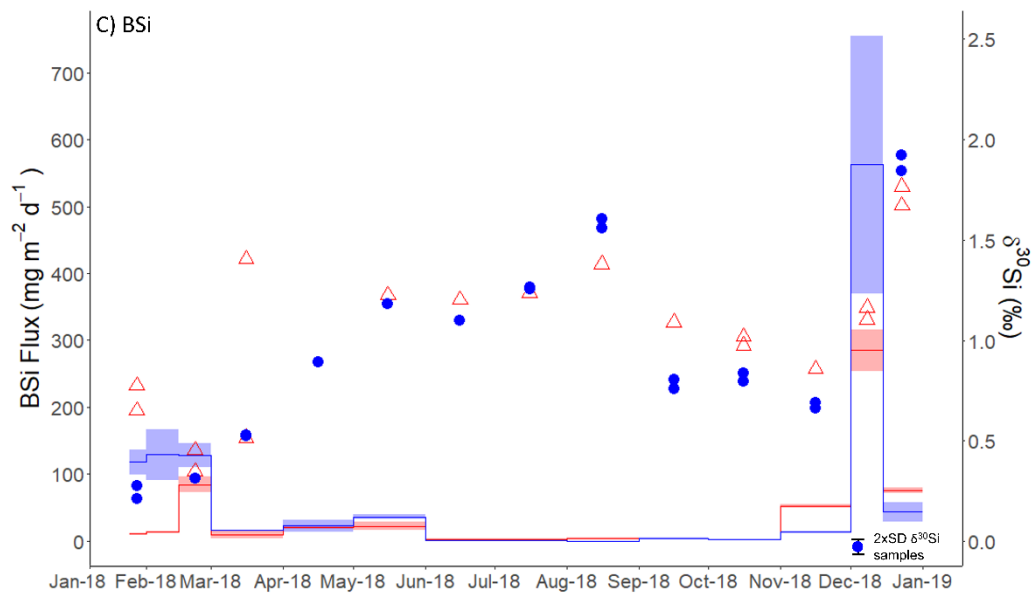
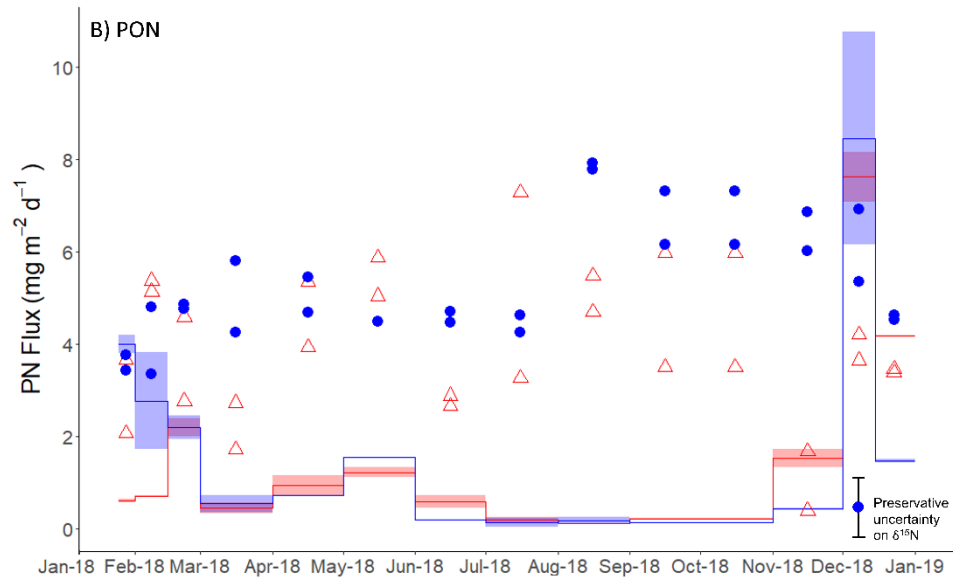
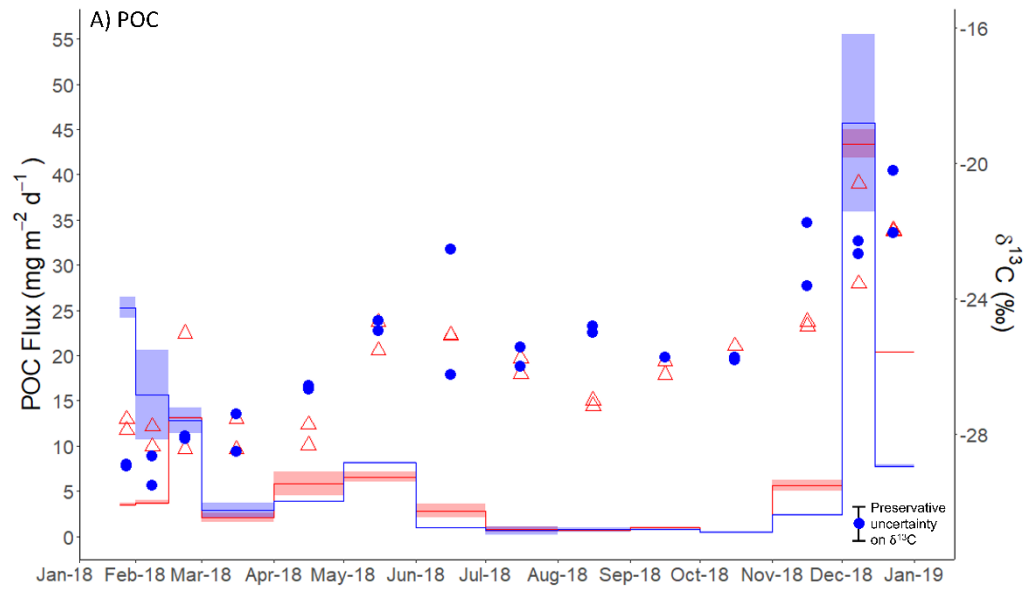
319 3.2. POC, PN, BSi fluxes

320 There is a clear seasonal cycle in POC, PN and BSi fluxes, all tracking each other well (Figure 3). Since  
 321 two to three splits were analysed from each sediment trap bottle, we refer here to the mean flux for  
 322 each sediment trap bottle based on the available splits for that bottle. POC fluxes were low during  
 323 austral autumn and winter, with mean fluxes  $<10 \text{ mg C m}^{-2} \text{ d}^{-1}$  and  $<7 \text{ mg C m}^{-2} \text{ d}^{-1}$  for shallow and  
 324 deep traps respectively during the period March to October 2018. Higher fluxes were measured in  
 325 summer 2018 (productive period 1), reaching means of  $25.3 \text{ mg C m}^{-2} \text{ d}^{-1}$  in late January 2018 in the  
 326 shallow trap and  $13.1 \text{ mg C m}^{-2} \text{ d}^{-1}$  in late February in the deep trap. The maximum POC fluxes  
 327 measured occurred in early December 2018 (productive period 2), reaching with mean POC fluxes of  
 328  $45.7 \text{ mg C m}^{-2} \text{ d}^{-1}$  and  $43.4 \text{ mg C m}^{-2} \text{ d}^{-1}$ , in shallow and deep traps respectively. PN fluxes follow the  
 329 same trends as POC fluxes, peaking at  $4.2$  and  $2.4 \text{ mg N m}^{-2} \text{ d}^{-1}$  during period 1, and  $10.8$  and  $8.2 \text{ mg}$   
 330  $\text{N m}^{-2} \text{ d}^{-1}$  during period 2, in shallow and deep traps respectively (Figure 3B). The mean POC:PN ratio  
 331 (mol:mol) throughout the study period was  $6.40 (\pm 0.73)$  and  $6.02 (\pm 0.90)$  in shallow and deep traps  
 332 respectively with higher ratios in the productive periods compared to the winter months. Mean  
 333 POC:PN ratios were  $6.75 (\pm 0.46)$  and  $6.63 (\pm 0.71)$  during period 1 and period 2 in the shallow trap,  
 334 and  $6.61 (\pm 0.65)$  and  $5.51 (\pm 0.87)$  in the deep trap. Over the winter months POC:PN was  $5.68$  and  
 335  $5.92$  in shallow and deep traps respectively.

336

337 BSi fluxes (Figure 3C) track those of POC well. Lowest fluxes ( $<20 \text{ mg SiO}_2 \text{ m}^{-2} \text{ d}^{-1}$ , except a small peak  
338 of up to  $39.7 \text{ mg SiO}_2 \text{ m}^{-2} \text{ d}^{-1}$  in May 2018) occurred in the autumn/winter (March-October). During  
339 summer 2018 (productive period 1), BSi fluxes were high, reaching ~~mean fluxes of~~  $129.1 \text{ mg SiO}_2 \text{ m}^{-2}$   
340  $\text{d}^{-1}$  in early February in the shallow trap and  $84.3 \text{ mg SiO}_2 \text{ m}^{-2} \text{ d}^{-1}$  in late February in the deep trap. By  
341 far the highest fluxes were observed in spring 2018 (productive period 2), peaking in early December  
342 at ~~a mean of~~  $562.4 \text{ mg SiO}_2 \text{ m}^{-2} \text{ d}^{-1}$ , and  $285.4 \text{ mg SiO}_2 \text{ m}^{-2} \text{ d}^{-1}$  in shallow and deep traps respectively.  
343 The mean BSi:POC ratio (mol:mol) throughout the study period was  $29.82 (\pm 17.80)$  and  $25.86$   
344  $(\pm 11.72)$  in shallow and deep traps respectively. Higher BSi:POC ratios were observed in the shallow  
345 trap in period 1 ( $38.45 \pm 10.96$ ), and both shallow and deep traps in period 2 ( $36.94 \pm 16.32$  and  $35.70$   
346  $\pm 12.10$  respectively). BSi:POC ratios were lower in the deep trap during period 1 ( $23.64 (\pm 6.82)$ ).

347 The match in timing of ~~sharp peaks~~ elevated fluxes of POC, PN and BSi fluxes in the shallow and  
348 deep traps in spring (period 2) highlights that sinking rates must be sufficient ( $>114 \text{ m d}^{-1}$ ) for  
349 particles to travel the 1600 m between the two traps in the 14 day period that the sediment  
350 trap cups were open. In period 1, there was a time lag of 14 to 35 days ~~(based on the sampling~~  
351 ~~duration of each sample bottle was open)~~ between the timing of the maximum POC, PN, and BSi  
352 fluxes in the deep and shallow sediment traps. This suggests sinking rates of  $46\text{-}114 \text{ m d}^{-1}$ . However,  
353 we stress that this assumes vertical sinking, which as we discuss in ~~the~~ Section 4 is not always the  
354 case.



356

357 **Figure 3: A) Particulate organic carbon (POC), B) particulate nitrogen (PN) and C) biogenic silica**  
 358 **(SiO<sub>2</sub>, BSi) fluxes (mg m<sup>-2</sup> d<sup>-1</sup>) at deep (red shading) and shallow (blue shading) sediment traps.**  
 359 **Shading indicates the maximum and minimum flux from two replicate splits-samples, with the solid**  
 360 **line indicating the mean value. Coloured points show isotope ratios for A) δ<sup>13</sup>C<sub>POC</sub>, B) δ<sup>15</sup>N<sub>PN</sub> and C)**  
 361 **δ<sup>30</sup>Si<sub>BSi</sub> with red open triangles and blue filled circles indicating deepshallow and shallowdeep**  
 362 **sediment traps, respectively. The maximum error on sediment trap δ<sup>13</sup>C<sub>POC</sub> (±1‰) and δ<sup>15</sup>N<sub>PN</sub> (±1.5**  
 363 **‰) values are shown by scaled error bars in the bottom right corner, and are associated with**  
 364 **formaldehyde preservation (Mincks et al., 2008) since this vastly exceeds analytical error. For**  
 365 **δ<sup>30</sup>Si<sub>BSi</sub>, the scaled error bar represents 2 x SD (‰0.7) for the analytical sample replicates. For each**  
 366 **sample, ~~fluxes and~~ isotope ratios are given at the midpoint of the period date that the sample cup**  
 367 **was opened.**

368 3.3. δ<sup>13</sup>C<sub>POC</sub>, δ<sup>15</sup>N<sub>PN</sub> and δ<sup>30</sup>Si<sub>BSi</sub> Isotopes

369 δ<sup>13</sup>C<sub>POC</sub> values of deep and shallow sediment trap samples track each other well and show the same  
 370 order of enrichment and /depletion (Figure 3A). Again, when presenting the results for an individual  
 371 sediment trap bottle, we give the mean of replicate splits from that sediment trap bottle unless  
 372 otherwise stated. Initially, from January to March 2018, we see isotopically light ~~mean~~ δ<sup>13</sup>C<sub>POC</sub> values  
 373 between -27.40 and -28.56‰, before increasing to -24.38‰ and -25.07‰ in June in shallow and  
 374 deep traps respectively. Over winter, δ<sup>13</sup>C<sub>POC</sub> became more depleted (shallow: -25.76‰ in October,  
 375 deep -27.07‰ in August) with a slight divergence (2.17‰) in the tracking of deep and shallow  
 376 δ<sup>13</sup>C<sub>POC</sub> in August 2018. Coinciding with increasing chlorophyll concentrations, δ<sup>13</sup>C<sub>POC</sub> became more  
 377 enriched during the period September to December 2018 (-25.72 to -21.13‰ and -26.04 to -21.98  
 378 ‰ for shallow and deep traps respectively).

379 Comparison of flux-weighted δ<sup>13</sup>C<sub>POC</sub> values confirms the carbon isotopic similarity of deep and  
 380 shallow traps, particularly during period 2 (Table 1). These results also highlight the baseline-shift in  
 381 both δ<sup>13</sup>C<sub>POC</sub> and δ<sup>30</sup>Si<sub>BSi</sub> between period 1 and period 2.

382 **Table 1: Sediment trap seasonal (Jan 2018-Dec 2018), period 1 (Jan 2018 – April 2018), and period**  
 383 **2 (Sept 2018-Dec 2018) flux-weighted mean δ<sup>13</sup>C<sub>POC</sub> (‰), δ<sup>15</sup>N<sub>PN</sub> (‰) and δ<sup>30</sup>Si<sub>BSi</sub> (‰) for shallow**  
 384 **(400 m) and deep (2000 m) traps. Given that the analytical conditions were the same for all**  
 385 **samples measured, we use the pooled variance over the applicable time period as a measure of**  
 386 **uncertainty on these mean isotopic ratios. Degrees of freedom (dof) are based on cups with**  
 387 **replicate isotopic measurements and are given in parentheses. ~~Maximum errors are based on~~**  
 388 **uncertainty associated with formaldehyde preservative and analytical sample replicate**

Time period	δ <sup>13</sup> C <sub>POC</sub> (‰)		δ <sup>15</sup> N <sub>PN</sub> (‰)		δ <sup>30</sup> Si <sub>BSi</sub> (‰)	
	Shallow	Deep	Shallow	Deep	Shallow	Deep
Seasonal	-25.15 ±0.49 <u>(dof=14)1‰</u>	-24.40 ±0.45 <u>(dof=14)‰</u>	2.07 ±0.34 <u>(dof=14)1.5‰</u>	0.39 ±0.43 <u>(dof=14)1.5‰</u>	0.50 ±0.09 <u>(dof=8)7‰</u>	0.86 ±0.100 <u>(dof=6)7‰</u>
Period 1	-28.30 ±0.314 <u>(dof=5)‰</u>	-27.52 ±0.33 <u>(dof=5)1‰</u>	1.16 ±0.36 <u>(dof=5)1.5‰</u>	0.73 ±0.58 <u>(dof=5)1.5‰</u>	0.25 ±0.09 <u>(dof=2)7‰</u>	0.47 ±0.130 <u>(dof=2)7‰</u>

Period 2	-22.47 ±1.03 (dof=5)‰	-22.79 ±0.74 (dof=5)1‰	2.97 ±0.66 (dof=5)1.5‰	-0.09 ±0.65 (dof=5)1.5‰	1.54 ±0.300 (dof=4)7‰	1.08 ±0.140 (dof=4)7‰
----------	--------------------------	---------------------------	---------------------------	----------------------------	--------------------------	--------------------------

389

390  $\delta^{15}\text{N}_{\text{PN}}$  values are less consistent between deep and shallow sediment trap samples and there is  
391 more heterogeneity between sample ~~split~~replicates. For the shallow trap we see values ranging  
392 between +0.13 and +2.96‰ (mean +1.42‰, SD 0.79‰) from January to June 2018, and, for the  
393 deep trap, values ranged between -1.95 and +3.04‰ (mean +0.60‰, SD 1.60‰) during this  
394 period. ~~There is no clear trend during this period, but shallow and deep traps have  $\delta^{15}\text{N}_{\text{PN}}$  of similar~~  
395 ~~magnitude.~~ Values increase between June and August, reaching ~~a mean of~~ +5.42 and +2.10‰ in  
396 shallow and deep traps respectively. From August to December (shallow), and August to November  
397 (deep), we see a trend of decreasing  $\delta^{15}\text{N}_{\text{PN}}$  to +1.49 and -2.77‰ in shallow and deep traps  
398 respectively, ~~with the decrease being of similar magnitude (3.93 and 4.87 respectively) for both~~  
399 ~~traps.~~ Shallow  $\delta^{15}\text{N}_{\text{PN}}$  are consistently higher than deep  $\delta^{15}\text{N}_{\text{PN}}$  by 4.52‰ on average during this  
400 period (August to November). In the deep trap we see a final increase in  $\delta^{15}\text{N}_{\text{PN}}$  coinciding with the  
401 increase in PN flux from November to December 2018, reaching a mean of +0.71‰. The same  
402 increase in  $\delta^{15}\text{N}_{\text{PN}}$  is not apparent in the shallow trap.

403 Si isotope compositions in deep and shallow samples were similar, exhibiting the same seasonal  
404 patterns. Both deep and shallow traps showed an increase in  $\delta^{30}\text{Si}_{\text{BSi}}$  from January to July 2018  
405 (+0.24 to +1.26‰) with the steepest increase occurring from March to May (Figure 3C). Sample  
406 ~~splits~~replicates generally showed good agreement with one exception during March 2018 when  
407 ~~duplicate samples~~sample splits from the deep sediment trap were +0.52 and +1.41‰, highlighting  
408 the heterogeneous nature of the sediment trap material. Isotopic values were then quite steady  
409 over winter until the end of August when  $\delta^{30}\text{Si}_{\text{BSi}}$  began to decrease steeply, reaching +0.68 and  
410 +0.86‰ in shallow and deep traps respectively in November 2018. Following this,  $\delta^{30}\text{Si}_{\text{BSi}}$  increased  
411 rapidly to +1.72 (deep) and +1.89‰ (shallow) coinciding with the large increase in BSi fluxes at this  
412 time.

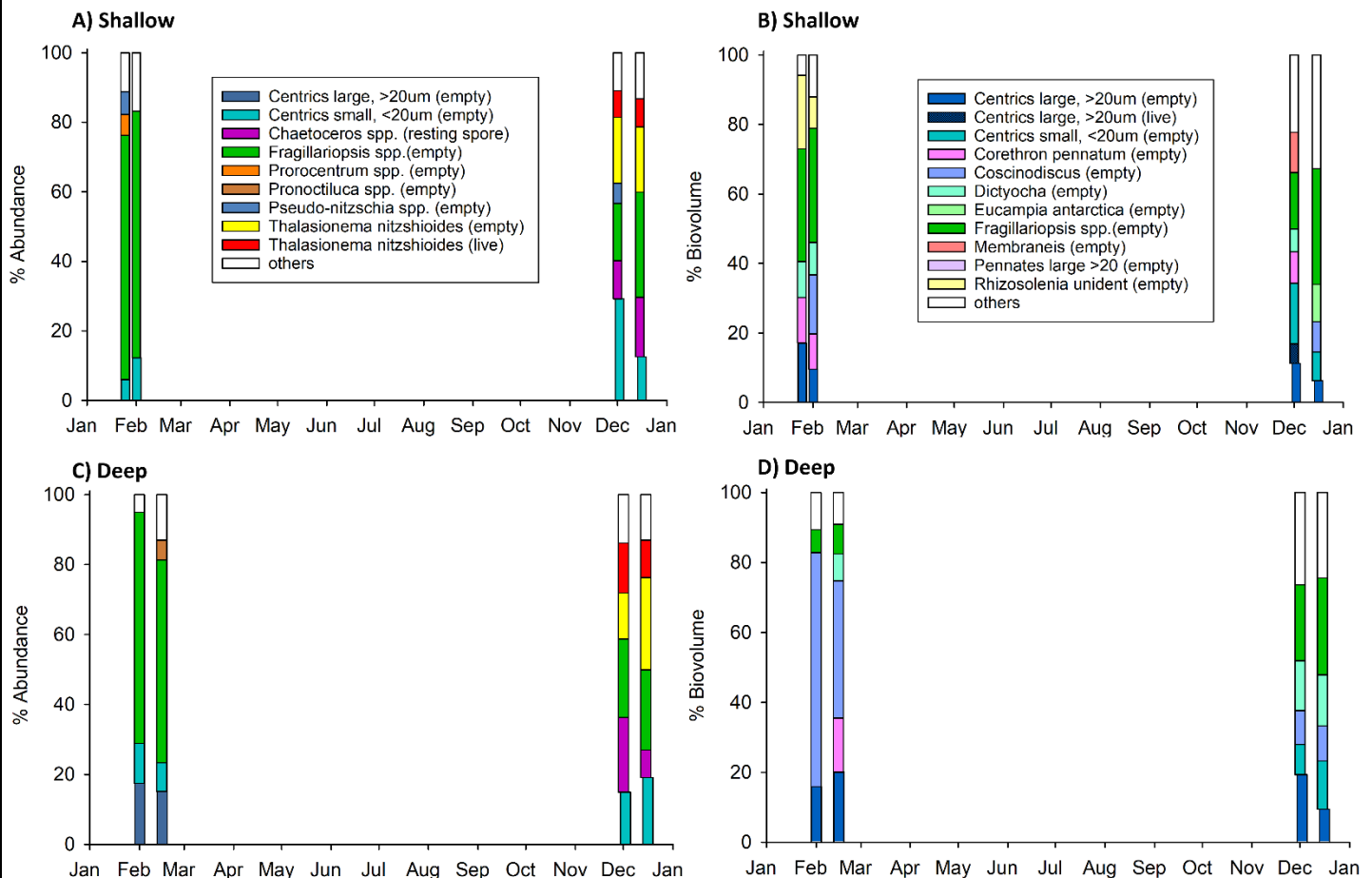
#### 413 3.4. Phytoplankton community structure

414 Eight samples (four deep and four shallow, [table 2](#)) were analysed ~~by light~~ microscopice ally for  
415 phytoplankton composition to cover the high productivity periods 1 and 2. ~~Diatoms, silicoflagellates~~  
416 ~~and dinoflagellates were observed, with a dominance of diatoms. Micro-zooplankton were also~~  
417 ~~recorded, in particular radiolarian and tintinnids, though these were not dominant by biovolume or~~  
418 ~~abundance.~~ Only intact cells were identified and counted. In terms of abundance, during period 1,  
419 ~~the diatoms~~ *Fragilariopsis spp.* dominated both deep (58-66%) and shallow (~70%) trap samples  
420 (Figure 4A, [CB](#)), whereas during period 2 the phytoplankton community structure was more mixed  
421 with contributions from ~~the diatoms~~ *Thalassionema nitzschiodes*, *Chaetoceros*, small (<20  $\mu\text{m}$ )  
422 centrics, as well as *Fragilariopsis spp.* Large centric ~~diatoms~~ (>20  $\mu\text{m}$ ) represented 15-20% of the  
423 community by abundance in the deep trap during productive period 1, but <2.5% in productive  
424 period 2. Interestingly we do not see these large centrics in the shallow trap during productive  
425 period 1, implying that sinking velocities were < 76  $\text{m d}^{-1}$  for these large phytoplankton cells ~~based on~~  
426 ~~the duration that the first sediment trap bottle was open and the depth between the two traps.~~

427 In terms of biovolume, *Fragilariopsis spp.* were still a dominant component of the shallow trap  
428 sample in period 1 (~33%) but were <9% of the community in the deep trap during period 1, with



429 the large cells of the diatom *Coscinodiscus* dominating 39-67% (Figure 4BC, D). Diatoms, *Corethron*  
 430 *pennatum* (shallow: 10-13%; deep: 15%), *Rhizosolenia* (shallow: 9-21%), and large centric diatoms  
 431 (>20 μm) (shallow: 10-17%; deep: 16-20%), as well as the silicoflagellate *Dictyocha* (shallow: 9-10  
 432 %; deep: 8%), were also relatively high in terms of biovolume during period 1. During period 2, the  
 433 community in terms of biovolume was quite mixed in the shallow trap (Figure 4BC), with similar  
 434 contributions from *Fragilariopsis* spp. (22-28%), *Dictyocha* (14-15%), *Coscinodiscus* (10%), and,  
 435 small (<20 μm, 9-14%) and large (>20 μm, 9-19%) centric diatoms (>20 μm, 9-19%) in the deep trap.



437 **Figure 4: Phytoplankton assemblage of A,B) shallow and C, D) deep sediment trap samples**  
 438 **according to abundance (A, C) and biovolume (B, D). Four samples were taxonomically identified**  
 439 **for each trap. Shown here are the Plots A and C show phytoplankton contributing >5% by**  
 440 **abundance, and (A,B) or plots B and D show >5% by biovolume (C,D). Four samples were**  
 441 **taxonomically identified taxonomically for each trap. Note that only intact cells were counted.**

442

#### 443 4. Discussion

444 In this study we measure the seasonal cycle of POC, PN and BSi fluxes as well as the  $\delta^{13}\text{C}_{\text{POC}}$ ,  $\delta^{15}\text{N}_{\text{PN}}$   
445 and  $\delta^{30}\text{Si}_{\text{BSi}}$  values of sinking particles collected in shallow (400 m) and deep (2000 m) sediment traps  
446 in the Scotia Sea, Southern Ocean. Both the magnitude and isotopic compositions were generally  
447 similar in the shallow and deep sediment traps, suggesting that most remineralisation occurred in  
448 the upper 400 m. This highlights that material reaching 400 m likely facilitates the transfer of carbon  
449 much deeper in the ocean, sequestering carbon for longer time periods ([Kwon et al., 2009](#)).

##### 450 4.1. Seasonal flux cycles

451 [The seasonal cycles of POC agree well with previously published work at the same location \(Manno](#)  
452 [et al., 2015\)](#), with peaks in austral spring and late summer, though the peak POC fluxes recorded  
453 here (~~means of~~ 45.7 mg C m<sup>-2</sup> d<sup>-1</sup> and 43.4 mg C m<sup>-2</sup> d<sup>-1</sup>, in shallow and deep traps respectively) are  
454 higher than those observed in previous years (22.9 mg C m<sup>-2</sup> d<sup>-1</sup>; Manno et al. (2015)). A smaller  
455 ~~additional third~~ peak in POC flux (<10 mg C m<sup>-2</sup> d<sup>-1</sup>) occurred in April/May, in agreement with some  
456 previous years (Manno et al., 2015). PN fluxes followed the same seasonal trend as POC [for both](#)  
457 [deep and shallow traps suggesting a similar source. The similar magnitude of POC:PN ratios in period](#)  
458 [1 in the two traps support consistency in the degree of degradation at these depths. The lower](#)  
459 [POC:PN ratios measured in the deep trap between August and October, compared to the shallow](#)  
460 [trap are consistent with a divergence in  \$\delta^{15}\text{N}\_{\text{PN}}\$  ratios, and could relate to a change in source material](#)  
461 [and/or degradation state between the two traps at this time.](#)

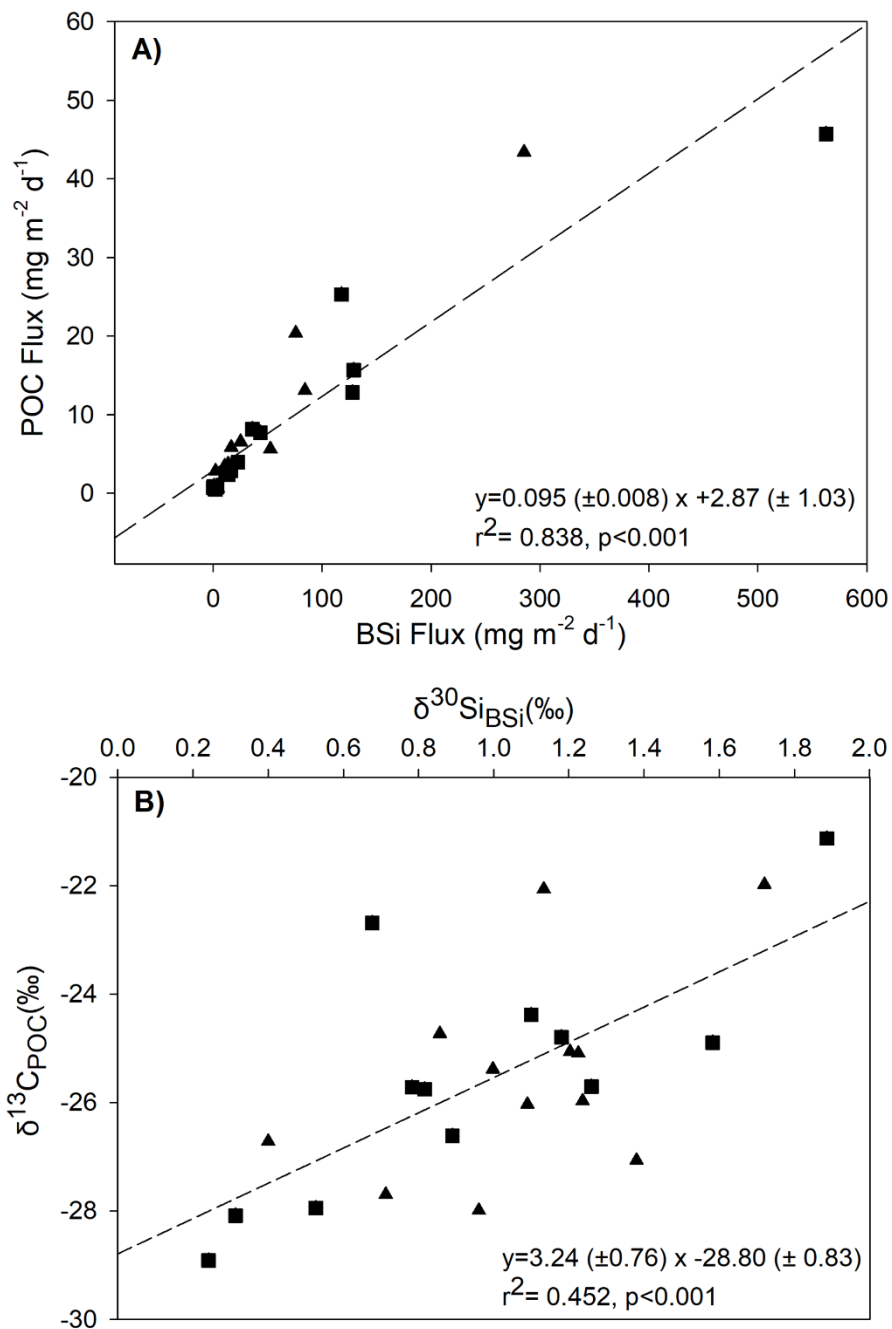
462 ~~Our measured~~ [The fluxes of BSi observed here](#) are higher than previously observed at this site at  
463 2000 m in 2012 (Rembauville et al., 2016). Maximum fluxes of 46.0 mg SiO<sub>2</sub> m<sup>-2</sup> d<sup>-1</sup> were recorded by  
464 Rembauville et al. (2016) in January 2012, which though of similar magnitude to our summer peak of  
465 84.3 mg SiO<sub>2</sub> m<sup>-2</sup> d<sup>-1</sup>, is an order of magnitude lower than the spring peak of 285.4 mg SiO<sub>2</sub> m<sup>-2</sup> d<sup>-1</sup> in  
466 December 2018. However, the Rembauville et al. (2016) record ends in November and therefore  
467 would not have captured the main peak in particle flux following the phytoplankton spring bloom in  
468 December (apparent in satellite surface chlorophyll, Figure 2 in Rembauville et al. (2016)).  
469 ~~Additionally, we do not capture the first 3 weeks of January in our data.~~ Closset et al. (2015)  
470 measured very high fluxes (>700 mg SiO<sub>2</sub> m<sup>-2</sup> d<sup>-1</sup>) of BSi south of the Polar Front in the Australian  
471 sector of the Southern Ocean at 2000 m, and similarly high fluxes have been observed in other  
472 sectors (Fischer et al., 2002; Honjo et al., 2000).

473 We define two main productive periods, productive period 1 from January to April 2018, and  
474 productive period 2 from September to December 2018 when chlorophyll concentrations were >0.4  
475 mg m<sup>-3</sup>. [Satellite data suggest the magnitude of chlorophyll concentration was similar during both](#)  
476 [productive periods, but increasing in magnitude throughout period 2, and decreasing in period 1,](#)  
477 [consistent with timing of sampling.](#) The particle fluxes associated with productive period 2 were  
478 much higher than those during productive period 1, a difference which is particularly pronounced for  
479 BSi fluxes. The bloom during period 2 was more geographically widespread (Figure S2) and thus it is  
480 possible that if more of the material reaching the trap was sourced from productive waters, this  
481 could have supported the higher fluxes observed at this time. The observed higher BSi fluxes in  
482 productive period 2 could also relate to ~~the~~ [the presence of more heavily silicified diatom species at](#)  
483 [this time, including the occurrence of resting spores \(\*Chaetoceros spp.\*; Figure 4, and Rembauville et](#)  
484 [al. \(2016\)\), increased aggregation \(and thus sinking\) potential, higher sinking rates, and/or reduced](#)

485 grazing pressure. The fact that we observed resting spores at the end of productive period 2,  
486 suggests that nutrients may have started to become limiting for at least some of the phytoplankton  
487 community (e.g. silicic acid and/or iron, (Rembauville et al., 2016)). ~~Satellite data suggest the~~  
488 ~~magnitude of chlorophyll concentration was similar during both productive periods, but increasing in~~  
489 ~~magnitude throughout period 2, and decreasing in period 1.~~ POC and BSi fluxes track each other  
490 closely and ratios suggest high export of biogenic silica (Figure 5). This, ~~which,~~ combined with our  
491 visual observations of a dominance of algal material in the trap during the spring peak that was  
492 ~~(dominated by diatoms, (Figure 4),~~ highlight suggest an important role for ~~s the role of~~ diatoms in  
493 transferring organic carbon to the deep ocean at this time. This could be achieved if cells are large  
494 through large mineral (silica) ballasted cells sinking at high velocities (Baumann et al., 2022), their  
495 greater density, and thus sinking velocities, associated with mineral (silica) ballast, or through the  
496 bioprotection of internal organic matter from grazing and oxidation by the diatom silica frustules  
497 (Passow and De La Rocha, 2006; Armstrong et al., 2001; Smetacek et al., 2004).

#### 498 4.2. Seasonal *variation shifts* in isotope ratios

499 In terms of the seasonality, we see broadly similar trends for both  $\delta^{13}\text{C}_{\text{POC}}$  and  $\delta^{30}\text{Si}_{\text{BSi}}$  (linear  
500 regression,  $R^2 = 0.452$ ,  $pP < 0.001$ , Figure 5), again highlighting the close coupling of carbon and silicon  
501 cycling processes. We do not find significant relationships between  $\delta^{15}\text{N}_{\text{PN}}$  and  $\delta^{13}\text{C}_{\text{POC}}$  or  $\delta^{30}\text{Si}_{\text{BSi}}$ . We  
502 break the season into 3 main periods for discussion, productive period 1 (first export event), the  
503 winter flux hiatus, and productive period 2 (second export event).



504

505 Figure 5: Relationship between BSi and POC for data from both deep (triangles) and shallow  
 506 (squares) sediment traps. A) Regression between BSi and POC fluxes, and B-) between  $\delta^{13}\text{C}_{\text{POC}}$  and  
 507  $\delta^{30}\text{Si}_{\text{BSi}}$ . Regression lines are shown by dotted lines with coefficients and associated standard errors  
 508 also shown.

509

510 4.2.1. Productive period 1

511

512 In terms of the seasonality, we see broadly similar trends for both  $\delta^{13}\text{C}_{\text{POC}}$  and  $\delta^{30}\text{Si}_{\text{BSi}}$  (linear  
513 regression,  $R^2 = 0.452$ ,  $P < 0.001$ ), again highlighting the close coupling of carbon and silicon cycling  
514 processes. During productive period 1,  $\delta^{13}\text{C}_{\text{POC}}$  is low, averaging  $-28.30$  and  $-27.52$  ‰ in shallow and  
515 deep traps respectively, close to that expected for Southern Ocean phytoplankton employing typical  
516 C3 metabolism (i.e. diffusive  $\text{CO}_2$  transfer into the internal cell pool and Rubisco carboxylation)  
517 (Raven, 1997). This is supported by consistent with the dominance of diatoms (*Fragilariopsis spp.*) in  
518 the trap material, as Bacillariophyceae are known to employ C3 metabolism (Table IV in Raven,  
519 1997). Preferential uptake of  $^{28}\text{Si}$  by diatoms (De La Rocha et al., 1997) during the late spring bloom  
520 of productive period 1, also explains the low  $\delta^{30}\text{Si}_{\text{BSi}}$  values. BSi:POC ratios were elevated at the start  
521 of productive period 1, suggesting that phytoplankton were heavily silicified. After initial low values,  
522 we see a progressive increase in both  $\delta^{13}\text{C}_{\text{POC}}$  and  $\delta^{30}\text{Si}_{\text{BSi}}$ , reflecting the progressive utilisation of both  
523  $^{12}\text{C}$  and  $^{28}\text{Si}$  as nutrient pools are consumed during the bloom. As such, the diatom cells reaching the  
524 sediment trap in late spring/summer were utilising increasingly isotopically-enriched C and Si for  
525 growth leading to progressive isotopic enrichment of the cells sinking into the sediment trap. This  
526 observation fits with elevated but decreasing surface chlorophyll concentrations from February to  
527 April 2018. Increasing  $\delta^{13}\text{C}_{\text{POC}}$  and  $\delta^{30}\text{Si}_{\text{BSi}}$  into the late summer may also partially reflect preferential  
528 remineralisation of the more labile  $^{12}\text{C}$  and  $^{28}\text{Si}$  in particles as they sink through the upper 400 m of  
529 the water column. ~~I-Though~~ the lack of variation in  $\delta^{13}\text{C}_{\text{POC}}$  and  $\delta^{30}\text{Si}_{\text{BSi}}$  between 400 and 2000 m in  
530 our study suggests this may be limited over these depth ranges, or that there is no fractionation  
531 effect. Whilst laboratory-based silica dissolution experiments are equivocal (Demarest et al., 2009;  
532 Wetzel et al., 2014), our findings agree with field studies that also indicate a lack of Si isotopic  
533 fractionation during diatom silica dissolution (Closset et al., 2015; Egan et al., 2012).

534 ~~During the summer-autumn period (January-June 2018)~~ productive period 1, there was no clear  
535 trend in  $\delta^{15}\text{N}_{\text{PN}}$ , with values between  $-1.954$  and  $+23.9604$  ‰. We speculate that this mixed signal  
536 with no significant difference between deep and shallow traps resulted from a combination of  
537 surface phytoplankton using both ammonium and nitrate as the inorganic nitrogen source, and  
538 variability in the sediment trap material composition, for example the presence of faecal pellets, as  
539 well as animal moults and carcasses. Enrichments of 2-4 ‰ occur between successive trophic levels,  
540 and egestion and excretion can have varying isotopic effects (see Section 4.3), thus the presence of  
541 faecal pellets, animal moults and carcasses could alter the isotopic composition of the sediment trap  
542 material. Additionally, any supply of ammonium through remineralisation would be utilised quickly  
543 because ammonium is kinetically favourable to nitrate (Glibert et al., 2016), resulting in particles  
544 with a decreased  $\delta^{15}\text{N}_{\text{PN}}$  compared to those produced by nitrate assimilation.

545

#### 546 4.2.2. Winter hiatus

547 Between May and August, both  $\delta^{13}\text{C}_{\text{POC}}$  and  $\delta^{30}\text{Si}_{\text{BSi}}$  showed little change were consistent, with a slight  
548 progressive decrease for  $\delta^{13}\text{C}_{\text{POC}}$  and slight increase in  $\delta^{30}\text{Si}_{\text{BSi}}$ . It is possible that the slight progressive  
549 trend towards a lighter carbon isotopic composition of sinking particles from  $-24.94$  to  $-25.98$  ‰ is  
550 driven by a mixture of older, isotopically heavier particles that have undergone partial  
551 remineralisation and the input of fresher material of different isotopic composition from the small  
552 secondary peak in POC we observed in April/May. An input of smaller, more slowly sinking cells  
553 reaching the trap in increasing numbers following the initial late spring peak in production could  
554 drive the lower  $\delta^{13}\text{C}_{\text{POC}}$  at this time. Additionally, the pulse of material could be driven by a



555 [successive peak in production of a different phytoplankton community with a different isotopic](#)  
556 [signature](#). Either the small autumn peak consisted of a different phytoplankton community, or we  
557 [are seeing a signal of smaller, more slowly sinking cells reaching the trap in increasing numbers](#)  
558 [following the initial late spring peak in production](#). Korb et al. (2012) found an increasing presence of  
559 [dinoflagellates from spring to summer, as well as seasonal changes in the size structure of the](#)  
560 [phytoplankton community to the northwest of South Georgia, supporting either hypothesis](#). We do  
561 [not have the species composition data from this time period to evidence this directly, but we](#)  
562 [suggest that the reduction in  \$\delta^{13}\text{C}\_{\text{POC}}\$  does not relate to a mixing event and a resupply of  \$^{12}\text{C}\$ , due to](#)  
563 [the fact that  \$\delta^{30}\text{Si}\_{\text{BSi}}\$  continued to increase slowly](#). Given the generally lighter silicon isotopic  
564 [composition of seawater below the photic zone, we would expect a mixing event to also result in a](#)  
565 [decline in seawater  \$\delta^{30}\text{Si}\$  and consequently, so,  \$\delta^{30}\text{Si}\_{\text{BSi}}\$](#) . This would mean that our hypothesised shift  
566 [in phytoplankton species composition in the traps \(May-August\) did not impact Si fractionation to](#)  
567 [the same extent as carbon isotopes](#). Whereas size, growth rates, cell geometry and different carbon  
568 [acquisition mechanisms have all been highlighted as impacting the  \$\delta^{13}\text{C}\_{\text{POC}}\$  of marine plankton \(Popp](#)  
569 [et al., 1999, 1998; Bidigare et al., 1999; Trull and Armand, 2001; Tuerena et al., 2019\), species](#)  
570 [dependent Si fractionation by polar and subpolar diatoms has only been observed in the laboratory,](#)  
571 [not in the field \(Annett et al., 2017; Cassarino et al., 2017; Sutton et al., 2013\).](#)

572  [\$\delta^{15}\text{N}\_{\text{PN}}\$  in the shallow trap showed a slight progressive decrease over the winter period, before](#)  
573 [increasing in August to 5.42 ‰](#). The progressive decrease is consistent with the propagation of the  
574 [surface signal of phytoplankton growth and fractionation, with increasing influence of ammonium](#)  
575 [uptake as the season progresses that leads to low  \$\delta^{15}\text{N}\_{\text{PN}}\$](#) . The large range in  $\delta^{15}\text{N}_{\text{PN}}$  in the deep trap  
576 [in July makes it difficult to determine with certainty a trend in  \$\delta^{15}\text{N}\_{\text{PN}}\$  in the deep trap between July](#)  
577 [and October](#).

578

579

580 **Figure 5:**

581

582 ~~Between May and August, both  $\delta^{13}\text{C}_{\text{POC}}$  and  $\delta^{30}\text{Si}_{\text{BSi}}$  were consistent, with a slight progressive~~  
583 ~~decrease for  $\delta^{13}\text{C}_{\text{POC}}$  and slight increase in  $\delta^{30}\text{Si}_{\text{BSi}}$ . It is possible that the slight progressive trend~~  
584 ~~towards a lighter carbon isotopic composition of sinking particles from 24.94 to 25.98‰ is driven~~  
585 ~~by a mixture of older, isotopically heavier particles that have undergone partial remineralisation and~~  
586 ~~the input of fresher material from the small secondary peak in POC we observed in April/May. Either~~  
587 ~~the small autumn peak consisted of a different phytoplankton community, or we are seeing a signal~~  
588 ~~of smaller, more slowly sinking cells reaching the trap in increasing numbers following the initial late~~  
589 ~~spring peak in production. Korb et al. (2012) found an increasing presence of dinoflagellates from~~  
590 ~~spring to summer, as well as seasonal changes in the size structure of the phytoplankton community~~  
591 ~~to the northwest of South Georgia, supporting either hypothesis. We do not have the species~~  
592 ~~composition data from this time period to evidence this directly, but we suggest that the reduction~~  
593 ~~in  $\delta^{13}\text{C}_{\text{POC}}$  does not relate to a mixing event and a resupply of  $^{12}\text{C}$ , due to the fact that  $\delta^{30}\text{Si}_{\text{BSi}}$~~   
594 ~~continued to increase slowly. Given the generally lighter silicon isotopic composition of seawater~~  
595 ~~below the photic zone, we would expect a mixing event to also result in a decline in seawater  $\delta^{30}\text{Si}$~~   
596 ~~and, so,  $\delta^{30}\text{Si}_{\text{BSi}}$ . This would mean that our hypothesised shift in phytoplankton species composition~~

597 ~~in the traps (May–August) did not impact Si fractionation to the same extent as carbon isotopes.~~  
598 ~~Whereas size, growth rates, cell geometry and different carbon acquisition mechanisms have all~~  
599 ~~been highlighted as impacting the  $\delta^{13}\text{C}_{\text{POC}}$  of marine plankton (Popp et al., 1999, 1998; Bidigare et al.,~~  
600 ~~1999; Trull and Armand, 2001; Tuerena et al., 2019), species-dependent Si fractionation by polar and~~  
601 ~~subpolar diatoms has only been observed in the laboratory, not in the field (Annett et al., 2017;~~  
602 ~~Cassarino et al., 2017; Sutton et al., 2013).~~

603 ~~During the summer–autumn period (January–June 2018), there was no clear trend in  $\delta^{15}\text{N}_{\text{PN}}$ , with~~  
604 ~~values between -1.94 and +3.04‰. We speculate that this mixed signal with no significant difference~~  
605 ~~between deep and shallow traps resulted from a combination of surface phytoplankton using both~~  
606 ~~ammonium and nitrate, and variability in the sediment trap material composition, for example the~~  
607 ~~presence of faecal pellets, as well as animal moults and carcasses. Enrichments of 2–4‰ occur~~  
608 ~~between successive trophic levels, and egestion and excretion can have varying isotopic effects (see~~  
609 ~~Section 4.3). Additionally, any supply of ammonium through remineralisation would be utilised~~  
610 ~~quickly because ammonium is kinetically favourable to nitrate (Glibert et al., 2016), resulting in~~  
611 ~~particles with a decreased  $\delta^{15}\text{N}_{\text{PN}}$  compared to those produced by nitrate assimilation.~~

#### 612 4.2.3. Productive period 2

613 At the start of productive period 2 (September) ~~Between August and September~~ we saw a  
614 significant ~~sharp~~ decrease in  $\delta^{30}\text{Si}_{\text{BSi}}$  (~0.5‰) in both traps suggesting resupply of  $^{28}\text{Si}$  enriched silicic  
615 acid to the euphotic zone via mixing. Interestingly, we did not see the same consistent shift in  
616 carbon isotopes; we measured a ~1‰ decrease in the shallow trap  $\delta^{13}\text{C}_{\text{POC}}$  and a ~1‰ increase in  
617 the deep trap  $\delta^{13}\text{C}_{\text{POC}}$ . We speculate that this mixing could bring waters of increased silicic acid  
618 concentrations to the surface, promoting full expression of the isotope fractionation effect enabling  
619 fractionation from phytoplankton uptake and supporting thus lower  $\delta^{30}\text{Si}_{\text{BSi}}$  in sinking particles. To  
620 match our observations, these mixed waters would need to be following phytoplankton uptake, but  
621 that the mixed waters were similar in dissolved inorganic carbon concentrations and  $\delta^{13}\text{C}$ , which.  
622 This could relate to the depth of mixing and differences in the depth at which POC and BSi are  
623 remineralised (Friedrich and Rutgers van der Loeff, 2002; Weir et al., 2020). We note that current  
624 velocities recorded at this time were elevated (Figure S1), particularly in the deep trap, suggesting a  
625 shift in the surrounding velocity fields, which and ~~may also~~ have resulted in biased sample collection  
626 at this time through either over or under collection (Buesseler et al., 2007). Whereas  $\delta^{13}\text{C}_{\text{POC}}$   
627 progressively increased during productive period 2, from -25.88‰ in September to -21.56‰ at the  
628 end of December (mean of deep and shallow traps),  $\delta^{30}\text{Si}_{\text{BSi}}$  continued to decrease until November  
629 before showing a sudden increase from +0.74‰ to +1.80‰ at the end of the sampling period. This  
630 may suggest that  $\text{DSi}_i$  ~~(or co-limiting nutrients,)~~ was replete, and uptake could occur unhindered  
631 until November 2018 when very high rates of production and the associated high fluxes of BSi  
632 increased the demand for  $\text{DSi}_i$ , and led to enrichment of  $\delta^{30}\text{Si}$  in overlying waters and subsequently  
633 sinking siliceous phytoplankton. For carbon, uptake was sufficient from September 2018 to  
634 progressively deplete source waters ~~(and subsequent newly formed phytoplankton cells)~~ in  $^{12}\text{C}$ ,  
635 driving an increase in  $\delta^{13}\text{C}$  in surface waters and newly formed phytoplankton cells. BSi:POC ratios  
636 increased from September to December suggesting that material reaching the traps was increasingly  
637 silicified.

638  $\delta^{15}\text{N}_{\text{PN}}$  decreased progressively from August to December ~~The progressive decrease is consistent with~~  
639 the propagation of the surface signal of phytoplankton growth and fractionation, with increasing

640 ~~influence of ammonium uptake that leads to low  $\delta^{15}\text{N}_{\text{PN}}$ , though the deep sediment trap showed a~~  
641 ~~sharp increase from a mean of -2.77 to +0.71‰ at the start of December, before decreasing again.~~  
642 ~~The progressive decrease is consistent with the propagation of the surface signal of phytoplankton~~  
643 ~~growth and fractionation, with increasing influence of ammonium uptake that leads to low  $\delta^{15}\text{N}_{\text{PN}}$ .~~  
644 Interestingly, unlike C and Si isotopes, we saw a divergence in the nitrogen isotopic composition of  
645 deep and shallow traps ~~during this period between August and December. Though they mostly~~  
646 ~~followed the same decreasing trend, the trend in the shallow trap was less pronounced and started~~  
647 ~~from a higher mean value of +5.42‰.~~ The sharp increase in mean  $\delta^{15}\text{N}_{\text{PN}}$  from +1.32‰ in July to  
648 +5.42‰ in August 2018 in the shallow trap that initiated the divergence strongly suggests an  
649 advective change in source material. As noted above, this was a period of increased horizontal  
650 velocities and may have facilitated material reaching the two traps from different sources of  
651 differing initial composition and degradation states. The substantially lower  $\delta^{15}\text{N}_{\text{PN}}$  in the deep trap  
652 from August to November, compared to that of the shallow trap is surprising. ~~It would be expected,~~  
653 ~~that, as particles sink and are progressively decomposed this would -given that we would expect~~  
654 ~~progressive decomposition of particles to -remove dissolved nitrogen depleted in  $^{15}\text{N}$ , thus~~  
655 ~~increasing. This would increase  $\delta^{15}\text{N}_{\text{PN}}$  in the particles, and indeed many studies have observed this~~  
656 ~~trend of increasing  $\delta^{15}\text{N}$  with depth in suspended particles (Altabet et al., 1991 and references~~  
657 ~~therein within).~~ However, like Altabet et al. (1991), we observe lower  $\delta^{15}\text{N}_{\text{PN}}$  in sinking particles in the  
658 deep sediment trap. This has also been observed previously in Antarctic waters (Wada et al., 1987).  
659 Though the reason for this is not well understood (Sigman and Fripiat, 2019), it appears to be a  
660 consistent phenomenon. Particles in our deep trap must therefore be gaining light nitrogen or losing  
661 heavy nitrogen and could reflect a different source composition. In agreement with Altabet et al.  
662 (1991), we suggest that lateral transport of low  $\delta^{15}\text{N}_{\text{PN}}$  from a region of increased ammonium-based  
663 production could explain this, highlighting a difference in the source of sinking particles to the two  
664 traps. Altabet et al. (1991) also suggests that, since protein nitrogen is 3‰ higher than bulk  
665 nitrogen, the selective decomposition of protein could explain the decrease in  $\delta^{15}\text{N}$  with depth,  
666 though why this would not be the case also for suspended PN is unclear. We observe the greatest  
667 divergence in shallow and deep N isotope compositions during periods of low PN flux (Figure 3),  
668 consistent with the observations of Altabet et al. (1991)}, enabling a low flux of laterally supplied  
669 material to have an amplified impact on the isotope signal. In support of this, in December when  
670 particle fluxes increase sharply with the spring bloom,  $\delta^{15}\text{N}_{\text{PN}}$  in the deep trap increases more in line  
671 with that of the shallow trap, highlighting a switch from source material being dominated by lateral  
672 supply when vertical supply is negligible, to the dominance of vertical supply from surface  
673 production following the phytoplankton bloom.

674 ~~Though complex, it is clear that seasonal patterns in isotopic composition of particulate material~~  
675 ~~reaching the sediment traps closely reflects the degree and type of nutrient utilisation in the source~~  
676 ~~waters. As we capture two main productive periods in our study, we can more closely examine the~~  
677 ~~different isotopic baselines observed in these two periods.~~

#### 678 4.2.4.3. Drivers of a shifting isotopic baselines ratios

679 The mean flux-weighted isotopic composition measured during Pproductive periods 1 (January to  
680 April 2018) and 2 (September to December 2018) suggests that the processes driving the flux of  
681 material at these times differ exhibit differing baselines in their isotopic composition (Figure 3, Table  
682 1). The divergence in the  $\delta^{15}\text{N}_{\text{PN}}$  of deep and shallow trap material during period 2 limits our ability

683 to compare [the temporal shifts in mean isotopic ratio baselines](#) for nitrogen isotopes, so we focus  
684 here on  $\delta^{13}\text{C}_{\text{POC}}$  and  $\delta^{30}\text{Si}_{\text{BSi}}$ . Since our record does not extend beyond December 2018, [and we do](#)  
685 [not capture the first 3 weeks of January 2018 when fluxes are likely high, we do not record the initial](#)  
686 [value at this time, however, we would expect  \$\delta^{13}\text{C}\_{\text{POC}}\$  to be even more negative at this time. We we](#)  
687 cannot determine if  $\delta^{13}\text{C}_{\text{POC}}$  and  $\delta^{30}\text{Si}_{\text{BSi}}$  would return to values akin to that in period 1 in the  
688 following late spring-summer season (January 2019). We saw a shift in ~~the baseline~~  $\delta^{13}\text{C}_{\text{POC}}$  from a  
689 mean of  $-28.31\text{‰}$  [in January 2018 at the time of our first measurements in January 2018 at the start](#)  
690 [of period 1](#), to  $-25.88\text{‰}$  in September at the start of period 2. This coincided with a change in  
691 community structure, with abundance dominated by *Fragilariopsis spp.* in period 1 to a more mixed  
692 community in period 2. Of the abundant phytoplankton species (>5%, Figure 4A, [BC](#)), we find  
693 statistically significant linear relationships between  $\delta^{13}\text{C}_{\text{POC}}$  and percent abundance for *Fragilariopsis*  
694 *spp.* (empty:  $R^2 = 0.926$ ,  $p < 0.001$ ), *Thalassionema nitzschioides* (live:  $R^2 = 0.774$ ,  $p = 0.004$ ; empty:  $R^2$   
695  $= 0.844$ ,  $p = 0.001$ ), and *Chaetoceros spp. (resting spore)* ( $R^2 = 0.732$ ,  $p = 0.007$ ). We stress this is based  
696 on only 8 samples. [Nevertheless, these robust samples show that there was a shift in phytoplankton](#)  
697 [community structure.](#) Although *Fragilariopsis spp.* were mainly empty cells, colonisation by bacteria  
698 (Grossart et al., 2003; Kjørboe et al., 2003) may facilitate carbon transfer within and on these cells,  
699 and certainly the live cells of *T. nitzschioides* and resting spores of *Chaetoceros spp.* would act as  
700 agents of carbon transfer (Agusti et al., 2015; Salter et al., 2012; Rembauville et al., 2016).

701 We examine whether this shift in [phytoplankton](#) community composition is associated with a change  
702 in SA:V (Table 2) since greater fractionation of carbon in smaller phytoplankton cells with higher  
703 SA:V is well observed in the literature (e.g. Popp et al., 1998; Tuerena et al., 2019). There was a  
704 statistically significant (paired t-test,  $p = 0.008$ ) difference in the community SA:V between productive  
705 periods, increasing from  $0.35 \mu\text{m}^2 \mu\text{m}^{-3}$  in period 1 to  $0.51 \mu\text{m}^2 \mu\text{m}^{-3}$  in period 2. However, this would  
706 [result in increased isotopic fractionation](#) ~~act in opposition to the decreased baseline fractionation at~~  
707 [the start of period 2 compared to period 1 during period 2, in opposition to what we observed.](#) We  
708 note here, that as only intact cells were counted, the measured SA:V ratios may not fully [account](#)  
709 [for represent](#) the isotopic composition of the trap material due to the presence of fragmented  
710 material. It is possible that there was a change in the ~~mechanism~~ of carbon uptake with the  
711 more mixed phytoplankton community [in period 2](#) using  $\text{HCO}_3^-$  instead of  $\text{CO}_2$  or employing carbon  
712 concentrating mechanisms (CCMs), both of which would result in higher  $\delta^{13}\text{C}_{\text{POC}}$  than the diffusive  
713 uptake of  $\text{CO}_2$  via Rubisco (Raven, 1997; Cassar et al., 2004). Studies show that there is much  
714 diversity amongst diatoms in the use of CCMs and many are able to take up both  $\text{CO}_2$  and  $\text{HCO}_3^-$   
715 (Trimborn et al., 2009; Roberts et al., 2007; Shen et al., 2017; Young et al., 2016). We suggest that  
716 species driven differences in carbon uptake mechanisms account in part for the differing ~~baselines in~~  
717  $\delta^{13}\text{C}_{\text{POC}}$  that we observed [at the start of period 1 and period 2 during the two main productive](#)  
718 [periods.](#)

719 **Table 2: Phytoplankton cell community surface area to volume (SA:V) ratios measured in deep and**  
720 **shallow sediment traps for samples enumerated in both productive periods 1 and 2.**

Bottle open date	Depth	Period	Mean community SA:V
25/01/2018	Shallow	1	0.39
01/02/2018	Shallow	1	0.35
01/02/2018	Deep	1	0.33

15/02/2018	Deep	1	0.32
01/12/2018	Deep	2	0.53
01/12/2018	Shallow	2	0.48
15/12/2018	Deep	2	0.53
15/12/2018	Shallow	2	0.52

721

722 ~~The fact that we~~ also observed a ~~shifting baselines~~ shift in ~~the mean flux-weighted~~  $\delta^{30}\text{Si}_{\text{BSi}}$  ratios  
723 ~~(Table 1) between period 1 and period 2. ,and that, with~~ With the exception of one culture study  
724 ~~(Sutton et al., 2013), systematic species driven shifts in~~  $\delta^{30}\text{Si}_{\text{BSi}}$  fractionation have not been observed  
725 ~~(e.g., De La Rocha et al., 1997), suggest~~ings that there may be an additional driver of the changing  
726 isotopic ~~baselines-ratios~~ ~~we observed between the start of period 1 and period 2~~. Since, prior to our  
727 first measurements there had been a long-lasting phytoplankton bloom (Figure S2), we would expect  
728 production to have utilised much of the light  $^{28}\text{Si}$ , resulting in particles with enriched  $\delta^{30}\text{Si}_{\text{BSi}}$  reaching  
729 the trap in January 2018. However, we observe isotopically light mean values of +0.48‰ at the start  
730 of ~~sampling at the end of January period 1~~, suggesting that there must have been a resupply of  $^{28}\text{Si}$ .  
731 Physical mixing, bringing deep and benthic waters rich in nutrients, including iron, to the surface  
732 waters around South Georgia, are known to support the large blooms occurring downstream of  
733 South Georgia (Matano et al., 2020; Nielsdóttir et al., 2012) and could supply both  $^{12}\text{C}$ -enriched  
734 ~~dissolved inorganic carbon~~ and  $^{28}\text{Si}$ -enriched silicic acid. Additional nutrients could also be supplied  
735 to our study region by glacial discharge associated with isotopically light silicon isotopic signatures  
736 (Matano et al., 2020; Hatton et al., 2019), or benthic fluxes from shelf sediments, likely also releasing  
737 isotopically light DSi (Ng et al., 2020; Cassarino et al., 2020; Closset et al., 2022). Therefore, we  
738 suggest that low values (increased fractionation) of  $\delta^{13}\text{C}_{\text{POC}}$  and  $\delta^{30}\text{Si}_{\text{BSi}}$  during period 1, relate to  
739 increased nutrient availability enabling full expression of the isotopic fractionation and thus  
740 isotopically light particulate material to reach the sediment trap.

741 The ocean circulation in our study region is complex and variable on fine spatial and temporal scales,  
742 affecting horizontal and vertical velocities (e.g. Boehme et al., 2008). It is clear from the currents  
743 measured at the depths of our two traps (Figure S1), that both the direction and magnitude of the  
744 flow can vary ~~within and between~~ seasons ~~salty~~ and is not necessarily consistent between the two  
745 depths. There are thus potentially different source regions for material in the two traps at certain  
746 times of the year. We lack the full depth resolution of vertical and horizontal velocity fields and  
747 information on sinking rates to confirm this, but previous studies have highlighted variability in the  
748 locations of the Southern Antarctic Circumpolar Current Front and the Polar Front, as well as eddies  
749 generated from these fronts, in our study region (Moore et al., 1999; Boehme et al., 2008;  
750 Whitehouse et al., 1996). We suggest that variability in ocean current velocities could ~~drive-explain~~  
751 different isotopic ~~ratios~~ ~~baselines~~ in period 1 and 2, through the supply of material to the traps ~~from~~  
752 ~~a~~ different source region with differing nutrient and remineralisation regimes. ~~Different source~~  
753 ~~waters~~ ~~This~~ would impact nutrient availability including iron supply, uptake and recycling (Hawco et  
754 al., 2021; Ellwood et al., 2020), which in turn influences species composition, nutrient utilisation and  
755 uptake rates (e.g. Meyerink et al., 2019). ~~This highlights the importance of making synchronous, and~~  
756 ~~full depth resolution measurements of, physical processes such as current strength and direction, to~~  
757 ~~be able to distinguish between spatial and temporal drivers of shifts in species composition, particle~~  
758 ~~flux and isotopic composition.~~



759 Since trophic transfer is known to impact both carbon and nitrogen isotope compositions of organic  
760 matter, the presence of moults and faecal pellets in trap samples are also important to consider. An  
761 incubation study focussed on *Euphausia superba* found that the  $\delta^{15}\text{N}$  of the *E. superba* faecal pellets  
762 was always lower than that of the copepods they ingested, though still higher than that of POM  
763 (Schmidt et al., 2003), ~~and~~ Additionally, Tamelander et al. (2006) measured faecal pellets produced  
764 by copepods with depleted  $^{15}\text{N}$  compared to the algal food source. Though a few studies on  
765 temperate and subtropical copepods showed that the faecal material had similar or slightly higher  
766  $\delta^{15}\text{N}$  than the food source (Altabet and Small, 1990; Checkley and Entzeroth, 1985), there is not a  
767 consistent fractionation effect of egestion, for either  $\delta^{15}\text{N}$  or  $\delta^{13}\text{C}$ , which may relate to compositional  
768 differences (protein, carbohydrate, lipid) and their isotopic values (Tamelander et al., 2006). We are  
769 therefore not able to determine the impact of faecal pellets or moults on the isotopic composition of  
770 our samples. As phytoplankton material dominated at the times of peak flux, we suggest that the  
771 importance of faecal pellets and moults may be greater during periods of lower flux, however we  
772 cannot rule out their contribution during the bloom periods. We suggest that it would be highly  
773 informative to conduct particle specific isotope analysis of common particle types in sediment traps  
774 such as faecal pellets, phytoplankton detritus and zooplankton moults, to improve our ability to  
775 determine the impact of particle flux composition on bulk isotope compositions.

776

## 777 SummaryConclusion

778 ~~We observed that the fluxes and isotopic ratios of sinking particulate material well represent the~~ The  
779 ~~seasonal cycles in primary productivity and nutrient uptake in surface waters at our study site in the~~  
780 ~~Scotia Sea~~ are reflected in the fluxes and isotopic ratios of sinking particulate material. We find that,  
781 ~~at our study site,~~ most remineralisation occurs in the upper 400 m of the water column, and below  
782 this the magnitude of the flux of sinking material is relatively consistent, supported by consistency in  
783 POC:PON ratios. ~~material is altered relatively little. This suggests that particles reaching 400 m likely~~  
784 ~~facilitate the transfer of carbon much deeper in the ocean, sequestering carbon for longer time~~  
785 ~~periods.~~ We find that particulate fluxes of C, N and BSi are ~~tightly~~ typically coupled which highlights  
786 the importance of siliceous material in the transfer of POC to depth. We suggest that a change in  
787 phytoplankton community structure can at least part explain the shifts in carbon isotopic  
788 composition between the two productive periods measured here, ~~and that the degree to which~~  
789 ~~trends in bulk isotopic compositions are coupled provides information on nutrient and~~  
790 ~~remineralisation regimes, and associated shifts in phytoplankton community structure. Though~~  
791 complex, seasonal patterns in isotopic composition of particulate material reaching the sediment  
792 traps do reflect the degree and type of nutrient utilisation in the source waters. ~~We suggest that it~~  
793 ~~would be highly informative to conduct particle specific isotope analysis of common particle types in~~  
794 ~~sediment traps such as faecal pellets, phytoplankton detritus and zooplankton moults, to improve~~  
795 ~~our ability to determine the impact of particle flux composition on bulk isotope compositions.~~ Our  
796 data also ~~reveals the~~ suggests an importance of ~~the~~ laterally supplied ~~of~~ material to the sediment  
797 traps and ~~support~~ suggests seasonal differences in source regions. ~~This highlights the importance of~~  
798 ~~making synchronous, and full depth resolution measurements of, physical processes such as current~~  
799 ~~strength and direction, to be able to distinguish between spatial and temporal drivers of shifts in~~  
800 ~~species composition, particle flux and isotopic composition.~~ Our results highlight how, t ~~Through~~  
801 more detailed mechanistic understanding of the drivers of POC flux, and biogeochemical cycling, we

802 can improve estimates of the current and future strength of the [biological carbon pump-BCP](#) and the  
803 ocean's role as a CO<sub>2</sub> sink.

804

#### 805 **Data availability**

806 Phytoplankton abundances and biovolume, as well as mean flux and isotopic ratios are available  
807 with the following DOI's:

808 DOI in progress with the British Antarctic Survey Polar Data Centre

#### 809 **Author contributions**

810 AB and CM conceived the study and participated in fieldwork to collect samples. AB conducted  
811 laboratory analysis with support from TW, LF, and UD for isotope analysis. MW conducted  
812 phytoplankton analysis and provided intellectual input on phytoplankton community composition.  
813 SH and KH provided support for isotopic analysis and contributed to the interpretation of the data  
814 and implications. [CC supported uncertainty analysis](#). All authors contributed text to the manuscript.

#### 815 **Competing Interests**

816 The authors declare that they have no conflict of interest.

817

#### 818 **Acknowledgements**

819 We are very grateful to the scientists and crew aboard research cruises JR17002 and DY098 for their  
820 efforts to deploy and recover the P3 mooring. We thank staff at the Bristol Isotope Group for  
821 running and maintenance of the mass spectrometer facilities at the University of Bristol, as well as  
822 Colin Chilcott for technical support for C and N analysis at the University of Edinburgh. AB and CM  
823 were supported by NC-ALI funding and ecosystems programme. CM was also funded by UKRI FLF  
824 project MR/T020962/1. SH was supported by the United Kingdom Natural Environment Research  
825 Council through grant NE/K010034/1. UD was supported by the UK NERC through grant  
826 NE/P006108/1. LF was supported by a NERC GW4+ DTP studentship and TW by a CSC-UoB Joint  
827 Scholarship. We thank Sally Thorpe and Emma Young for insights on the physical oceanographic  
828 conditions of the region. Finally, a special thanks to Flo Atherden for her dedicated work picking out  
829 swimmers from the shallow sediment trap.

830

#### 831 **References**

832 Agusti, S., González-Gordillo, J. I., Vaqué, D., Estrada, M., Cerezo, M. I., Salazar, G., Gasol, J. M., and  
833 Duarte, C. M.: Ubiquitous healthy diatoms in the deep sea confirm deep carbon injection by the  
834 biological pump, *Nat. Commun.*, 6, 1–8, <https://doi.org/10.1038/ncomms8608>, 2015.

835 Altabet, M. A. and Small, L. F.: Nitrogen isotopic ratios in fecal pellets produced by marine  
836 Zooplankton, *Geochim. Cosmochim. Acta*, 54, 155–163, [https://doi.org/10.1016/0016-](https://doi.org/10.1016/0016-7037(90)90203-W)  
837 [7037\(90\)90203-W](https://doi.org/10.1016/0016-7037(90)90203-W), 1990.

838 Altabet, M. A., Deuser, W. G., Honjo, S., and Stienen, C.: Seasonal and depth-related changes in the

839 source of sinking particles in the North Atlantic, *Nature*, 354, 136–139,  
840 <https://doi.org/10.1038/354136a0>, 1991.

841 Annett, A. L., Henley, S. F., Venables, H. J., Meredith, M. P., Clarke, A., and Ganeshram, R. S.: Silica  
842 cycling and isotopic composition in northern Marguerite Bay on the rapidly-warming western  
843 Antarctic Peninsula, *Deep. Res. Part II Top. Stud. Oceanogr.*, 139, 132–142,  
844 <https://doi.org/10.1016/j.dsr2.2016.09.006>, 2017.

845 Armstrong, R. A., Lee, C., Hedges, J. I., Honjo, S., and Wakeham, S. G.: A new, mechanistic model for  
846 organic carbon fluxes in the ocean based on the quantitative association of POC with ballast  
847 minerals, *Deep. Res. Part II Top. Stud. Oceanogr.*, 49, 219–236, [https://doi.org/10.1016/S0967-](https://doi.org/10.1016/S0967-0645(01)00101-1)  
848 [0645\(01\)00101-1](https://doi.org/10.1016/S0967-0645(01)00101-1), 2001.

849 Baumann, M., Joy Paul, A., Taucher, J., Thomas Bach, L., Goldenberg, S., Stange, P., Minutolo, F.,  
850 Riebesell, U., and Baumann mbaumann, M.: Drivers of Particle Sinking Velocities in the Peruvian  
851 Upwelling System, *EGU sphere. Prepr.*, 2022.

852 Belcher, A., Manno, C., Ward, P., Henson, S. A., Sanders, R., and Tarling, G. A.: Copepod faecal pellet  
853 transfer through the meso- and bathypelagic layers in the Southern Ocean in spring, *Biogeosciences*,  
854 14, <https://doi.org/10.5194/bg-14-1511-2017>, 2017.

855 Belcher, A., Manno, C., Thorpe, S., and Tarling, G.: Acantharian cysts: high flux occurrence in the  
856 bathypelagic zone of the Scotia Sea, Southern Ocean, *Mar. Biol.*, 165,  
857 <https://doi.org/10.1007/s00227-018-3376-1>, 2018.

858 Bidigare, R., Hanson, L., Buesseler, K. O., Wakeham, G., Freeman, H., Pancost, R. D., Millero, J.,  
859 Steinberg, P., Popp, N., Latasa, M., Landry, R., and Laws, A.: Iron-stimulated changes in <sup>13</sup>C  
860 fractionation and export by equatorial Pacific phytoplankton: Toward a paleogrowth rate proxy,  
861 *Paleoceanography*, 14, 589–595, <https://doi.org/10.1029/1999PA900026>, 1999.

862 Boehme, L., Meredith, M. P., Thorpe, S. E., Biuw, M., and Fedak, M.: Antarctic circumpolar current  
863 frontal system in the South Atlantic: Monitoring using merged Argo and animal-borne sensor data, *J.*  
864 *Geophys. Res.*, 113, C09012, <https://doi.org/10.1029/2007JC004647>, 2008.

865 Buesseler, K. O., Antia, A. N., Chen, M., Fowler, S. W., Gardner, W. D., Gustafsson, O., Harada, K.,  
866 Michaels, A. F., Rutgers van der Loeff, M., Sarin, M., Steinberg, D. K., and Trull, T.: An assessment of  
867 the use of sediment traps for estimating upper ocean particle fluxes, *J. Mar. Res.*, 65, 345–416,  
868 <https://doi.org/10.1357/002224007781567621>, 2007.

869 Cassar, N., Laws, E. A., Bidigare, R. R., and Popp, B. N.: Bicarbonate uptake by Southern Ocean  
870 phytoplankton, *Global Biogeochem. Cycles*, 18, 1–10, <https://doi.org/10.1029/2003GB002116>, 2004.

871 Cassarino, L., Hendry, K. R., Meredith, M. P., Venables, H. J., and De La Rocha, C. L.: Silicon isotope  
872 and silicic acid uptake in surface waters of Marguerite Bay, West Antarctic Peninsula, *Deep. Res. Part*  
873 *II Top. Stud. Oceanogr.*, 139, 143–150, <https://doi.org/10.1016/j.dsr2.2016.11.002>, 2017.

874 Cassarino, L., Hendry, K., Henley, S. F., Macdonald, E., Arndt, S., Freitas, F. S., Pike, J., and Firing, Y. L.:  
875 Sedimentary Nutrient Supply in Productive Hot Spots off the West Antarctic Peninsula Revealed by  
876 Silicon Isotopes, *Global Biogeochem. Cycles*, <https://doi.org/10.1029/2019GB006486>, 2020.

877 Checkley, D. M. and Entzeroth, L. C.: Elemental and isotopic fractionation of carbon and nitrogen by  
878 marine, planktonic copepods and implications to the marine nitrogen cycle, *J. Plankton Res.*, 7, 553–  
879 568, <https://doi.org/https://doi.org/10.1093/plankt/7.4.553>, 1985.

880 Closset, I., Cardinal, D., Bray, S. G., Thil, F., Djouaev, I., Rigual-Hernández, A. S., and Trull, T. W.:  
881 Seasonal variations, origin, and fate of settling diatoms in the Southern Ocean tracked by silicon  
882 isotope records in deep sediment traps, *Global Biogeochem. Cycles*, 29, 1495–1510,

883 <https://doi.org/10.1002/2015GB005180>, 2015.

884 Closset, I., Brzezinski, M. A., Cardinal, D., Dapoigny, A., Jones, J. L., and Robinson, R.: A silicon  
885 isotopic perspective on the contribution of diagenesis to the sedimentary silicon budget in the  
886 Southern Ocean, *Geochim. Cosmochim. Acta*, 327, 298–313, 2022.

887 Demarest, M. S., Brzezinski, M. A., and Beucher, C. P.: Fractionation of silicon isotopes during  
888 biogenic silica dissolution, *Geochim. Cosmochim. Acta*, 73, 5572–5583,  
889 <https://doi.org/10.1016/j.gca.2009.06.019>, 2009.

890 DeVries, T.: Atmospheric CO<sub>2</sub> and Sea Surface Temperature Variability Cannot Explain Recent  
891 Decadal Variability of the Ocean CO<sub>2</sub> Sink, *Geophys. Res. Lett.*, 49, 1–17,  
892 <https://doi.org/10.1029/2021GL096018>, 2022.

893 Egan, K. E., Rickaby, R. E. M., Leng, M. J., Hendry, K. R., Hermoso, M., Sloane, H. J., Bostock, H., and  
894 Halliday, A. N.: Diatom silicon isotopes as a proxy for silicic acid utilisation: A Southern Ocean core  
895 top calibration, *Geochim. Cosmochim. Acta*, 96, 174–192,  
896 <https://doi.org/10.1016/j.gca.2012.08.002>, 2012.

897 Ellwood, M. J., Strzeppek, R. F., Strutton, P. G., Trull, T. W., Fourquez, M., and Boyd, P. W.: Distinct  
898 iron cycling in a Southern Ocean eddy, *Nat. Commun.*, 11, 1–8, [https://doi.org/10.1038/s41467-020-](https://doi.org/10.1038/s41467-020-14464-0)  
899 [14464-0](https://doi.org/10.1038/s41467-020-14464-0), 2020.

900 Fischer, G., Gersonde, R., and Wefer, G.: Organic carbon, biogenic silica and diatom fluxes in the  
901 marginal winter sea-ice zone and in the Polar Front Region: Interannual variations and differences in  
902 composition, *Deep. Res. Part II Top. Stud. Oceanogr.*, 49, 1721–1745,  
903 [https://doi.org/10.1016/S0967-0645\(02\)00009-7](https://doi.org/10.1016/S0967-0645(02)00009-7), 2002.

904 Friedrich, J. and Rutgers van der Loeff, M. M.: A two-tracer (<sup>210</sup>Po-<sup>234</sup>Th) approach to distinguish  
905 organic carbon and biogenic silica export flux in the Antarctic Circumpolar Current, *Deep. Res. Part I*  
906 *Oceanogr. Res. Pap.*, 49, 101–120, [https://doi.org/10.1016/S0967-0637\(01\)00045-0](https://doi.org/10.1016/S0967-0637(01)00045-0), 2002.

907 Georg, R. B., Reynolds, B. C., Frank, M., and Halliday, A. N.: New sample preparation techniques for  
908 the determination of Si isotopic compositions using MC-ICPMS, *Chem. Geol.*, 235, 95–104,  
909 <https://doi.org/10.1016/j.chemgeo.2006.06.006>, 2006.

910 Giering, S. L. C., Cavan, E. L., Basedow, S. L., Briggs, N., Burd, A. B., Darroch, L. J., Guidi, L., Irisson, J.  
911 O., Iversen, M. H., Kiko, R., Lindsay, D., Marcolin, C. R., McDonnell, A. M. P., Möller, K. O., Passow, U.,  
912 Thomalla, S., Trull, T. W., and Waite, A. M.: Sinking Organic Particles in the Ocean—Flux Estimates  
913 From in situ Optical Devices, *Front. Mar. Sci.*, 6, <https://doi.org/10.3389/fmars.2019.00834>, 2020.

914 Gleiber, M. R., Steinberg, D. K., and Ducklow, H. W.: Time series of vertical flux of zooplankton fecal  
915 pellets on the continental shelf of the western Antarctic Peninsula, *Mar. Ecol. Prog. Ser.*, 471, 23–36,  
916 <https://doi.org/10.3354/meps10021>, 2012.

917 Glibert, P. M., Wilkerson, F. P., Dugdale, R. C., Raven, J. A., Dupont, C. L., Leavitt, P. R., Parker, A. E.,  
918 Burkholder, J. M., and Kana, T. M.: Pluses and minuses of ammonium and nitrate uptake and  
919 assimilation by phytoplankton and implications for productivity and community composition, with  
920 emphasis on nitrogen-enriched conditions, *Limnol. Oceanogr.*, 61, 165–197,  
921 <https://doi.org/10.1002/lno.10203>, 2016.

922 González, H. E., Daneri, G., Iriarte, J. L., Yannicelli, B., Menschel, E., Barría, C., Pantoja, S., and  
923 Lizárraga, L.: Carbon fluxes within the epipelagic zone of the Humboldt Current System off Chile: The  
924 significance of euphausiids and diatoms as key functional groups for the biological pump, *Prog.*  
925 *Oceanogr.*, 83, 217–227, <https://doi.org/10.1016/j.pocean.2009.07.036>, 2009.

926 Grasse, P., Brzezinski, M. A., Cardinal, D., De Souza, G. F., Andersson, P., Closset, I., Cao, Z., Dai, M.,

927 Ehlert, C., Estrade, N., François, R., Frank, M., Jiang, G., Jones, J. L., Kooijman, E., Liu, Q., Lu, D.,  
928 Pahnke, K., Ponzevera, E., Schmitt, M., Sun, X., Sutton, J. N., Thil, F., Weis, D., Wetzel, F., Zhang, A.,  
929 Zhang, J., and Zhang, Z.: GEOTRACES inter-calibration of the stable silicon isotope composition of  
930 dissolved silicic acid in seawater, *J. Anal. At. Spectrom.*, 32, 562–578,  
931 <https://doi.org/10.1039/c6ja00302h>, 2017.

932 Grasse, P., Haynert, K., Doering, K., Geilert, S., Jones, J. L., Brzezinski, M. A., and Frank, M.: Controls  
933 on the Silicon Isotope Composition of Diatoms in the Peruvian Upwelling, *Front. Mar. Sci.*, 8, 1–15,  
934 <https://doi.org/10.3389/fmars.2021.697400>, 2021.

935 Grossart, H. P., Kjørboe, T., Tang, K., and Ploug, H.: Bacterial colonization of particles: Growth and  
936 interactions, *Appl. Environ. Microbiol.*, 69, 3500–3509, [https://doi.org/10.1128/AEM.69.6.3500-](https://doi.org/10.1128/AEM.69.6.3500-3509.2003)  
937 [3509.2003](https://doi.org/10.1128/AEM.69.6.3500-3509.2003), 2003.

938 Hansman, R. L. and Sessions, A. L.: Measuring the in situ carbon isotopic composition of distinct  
939 marine plankton populations sorted by flow cytometry, *Limnol. Oceanogr. Methods*, 14, 87–99,  
940 <https://doi.org/10.1002/lom3.10073>, 2016.

941 Hasle, G. R. and Syvertsen, E. E.: Chapter 2 – Marine Diatoms, in: *Identifying Marine Phytoplankton*,  
942 edited by: Tomas, C. R., Academic Press, San Diego, 5–385, 1997.

943 Hatton, J. E., Hendry, K. R., Hawkings, J. R., Wadham, J. L., Opfergelt, S., Kohler, T. J., Yde, J. C., Stibal,  
944 M., and Žárský, J. D.: Silicon isotopes in Arctic and sub-Arctic glacial meltwaters: The role of  
945 subglacial weathering in the silicon cycle, *Proc. R. Soc. A Math. Phys. Eng. Sci.*, 475,  
946 <https://doi.org/10.1098/rspa.2019.0098>, 2019.

947 Hawco, N. J., Barone, B., Church, M. J., Babcock-Adams, L., Repeta, D. J., Wear, E. K., Foreman, R. K.,  
948 Björkman, K. M., Bent, S., Van Mooy, B. A. S., Sheyn, U., DeLong, E. F., Acker, M., Kelly, R. L., Nelson,  
949 A., Ranieri, J., Clemente, T. M., Karl, D. M., and John, S. G.: Iron Depletion in the Deep Chlorophyll  
950 Maximum: Mesoscale Eddies as Natural Iron Fertilization Experiments, *Global Biogeochem. Cycles*,  
951 35, 1–18, <https://doi.org/10.1029/2021GB007112>, 2021.

952 Hendry, K. R. and Brzezinski, M. A.: Using silicon isotopes to understand the role of the Southern  
953 Ocean in modern and ancient biogeochemistry and climate, *Quat. Sci. Rev.*, 89, 13–26,  
954 <https://doi.org/10.1016/j.quascirev.2014.01.019>, 2014.

955 Hendry, K. R. and Robinson, L. F.: The relationship between silicon isotope fractionation in sponges  
956 and silicic acid concentration: Modern and core-top studies of biogenic opal, *Geochim. Cosmochim.*  
957 *Acta*, 81, 1–12, <https://doi.org/10.1016/j.gca.2011.12.010>, 2012.

958 Henley, S. F., Annett, A. L., Ganeshram, R. S., Carson, D. S., Weston, K., Crosta, X., Tait, A., Dougan,  
959 J., Fallick, A. E., and Clarke, A.: Factors influencing the stable carbon isotopic composition of  
960 suspended and sinking organic matter in the coastal Antarctic sea ice environment, *Biogeosciences*,  
961 9, 1137–1157, <https://doi.org/10.5194/bg-9-1137-2012>, 2012.

962 Hillebrand, H., Dürselen, C. D., Kirschtel, D., Pollingher, U., and Zohary, T.: Biovolume calculation for  
963 pelagic and benthic microalgae, *J. Phycol.*, 35, 403–424, [https://doi.org/10.1046/j.1529-](https://doi.org/10.1046/j.1529-8817.1999.3520403.x)  
964 [8817.1999.3520403.x](https://doi.org/10.1046/j.1529-8817.1999.3520403.x), 1999.

965 Honjo, S., Francois, R., Manganini, S., Dymond, J., and Collier, R.: Particle fluxes to the interior of the  
966 Southern Ocean in the Western Pacific sector along 170°W, *Deep. Res. Part II*, 47, 3521–3548,  
967 [https://doi.org/10.1016/S0967-0645\(00\)00077-1](https://doi.org/10.1016/S0967-0645(00)00077-1), 2000.

968 Iversen, M. H., Pakhomov, E. A., Hunt, B. P. V., Jagt, H. Van Der, Wolf-gladrow, D., and Klaas, C.:  
969 Sinkers or floaters? Contribution from salp pellets to the export flux during a large bloom event in  
970 the Southern Ocean, *Deep Sea Res. Part II Top. Stud. Oceanogr.*, 138, 116–125,



971 <https://doi.org/10.1016/j.dsr2.2016.12.004>, 2017.

972 Kjørboe, T., Tang, K., Grossart, H. P., and Ploug, H.: Dynamics of microbial communities on marine  
973 snow aggregates: Colonization, growth, detachment, and grazing mortality of attached bacteria,  
974 *Appl. Environ. Microbiol.*, 69, 3036–3047, <https://doi.org/10.1128/AEM.69.6.3036-3047.2003>, 2003.

975 Korb, R. E., Whitehouse, M. J., Atkinson, A., and Thorpe, S.: Magnitude and maintenance of the  
976 phytoplankton bloom at South Georgia: a naturally iron-replete environment, *Mar. Ecol. Prog. Ser.*,  
977 368, 75–91, <https://doi.org/10.3354/meps07525>, 2008.

978 Korb, R. E., Whitehouse, M. J., Ward, P., Gordon, M., Venables, H. J., and Poulton, A. J.: Regional and  
979 seasonal differences in microplankton biomass, productivity, and structure across the Scotia Sea:  
980 Implications for the export of biogenic carbon, *Deep Sea Res. Part II Top. Stud. Oceanogr.*, 59–60,  
981 67–77, <https://doi.org/10.1016/j.dsr2.2011.06.006>, 2012.

982 Kwon, E., Primeau, F., and Sarmiento, J.: The impact of remineralization depth on the air-sea carbon  
983 balance, *Nat. Geosci.*, 2, 630–635, 2009.

984 De La Rocha, C. L., Brzezinski, M. A., and DeNiro, M. J.: Fractionation of silicon isotopes by marine  
985 diatoms during biogenic silica formation, *Geochim. Cosmochim. Acta*, 61, 5051–5056,  
986 [https://doi.org/10.1016/S0016-7037\(97\)00300-1](https://doi.org/10.1016/S0016-7037(97)00300-1), 1997.

987 Manno, C., Stowasser, G., Enderlein, P., Fielding, S., and Tarling, G. A.: The contribution of  
988 zooplankton faecal pellets to deep-carbon transport in the Scotia Sea (Southern Ocean),  
989 *Biogeosciences*, 12, 1955–1965, <https://doi.org/10.5194/bg-12-1955-2015>, 2015.

990 Manno, C., Fielding, S., Stowasser, G., Murphy, E. J., and Thorpe, S. E.: Continuous moulting by  
991 Antarctic krill drives major, *Nat. Commun.*, 16, 6051, <https://doi.org/10.1038/s41467-020-19956-7>,  
992 2020.

993 Matano, R. P., Combes, V., Young, E. F., and Meredith, M. P.: Modeling the Impact of Ocean  
994 Circulation on Chlorophyll Blooms Around South Georgia, Southern Ocean, *J. Geophys. Res. Ocean.*,  
995 125, 1–18, <https://doi.org/10.1029/2020JC016391>, 2020.

996 Medlin, L. K. and Priddle, J.: Polar marine diatoms, British Antarctic Survey, Cambridge, UK, 214 pp.,  
997 1990.

998 Meyerink, S. W., Boyd, P. W., Maher, W. A., Milne, A., Strzepek, R., and Ellwood, M. J.: Putting the  
999 silicon cycle in a bag: Field and mesocosm observations of silicon isotope fractionation in subtropical  
1000 waters east of New Zealand, *Mar. Chem.*, 213, 1–12,  
1001 <https://doi.org/10.1016/j.marchem.2019.04.008>, 2019.

1002 Michener, R. and Lajtha, K.: *Stable Isotopes in Ecology and Environmental Science: Second Edition*,  
1003 1–566 pp., <https://doi.org/10.1002/9780470691854>, 2008.

1004 Minagawa, M. and Wada, E.: Stepwise enrichment of  $^{15}\text{N}$  along food chains: Further evidence and  
1005 the relation between  $\delta^{15}\text{N}$  and animal age, *Geochim. Cosmochim. Acta*, 48, 1135–1140,  
1006 [https://doi.org/10.1016/0016-7037\(84\)90204-7](https://doi.org/10.1016/0016-7037(84)90204-7), 1984.

1007 Mincks, S. L., Smith, C. R., Jeffreys, R. M., and Sumida, P. Y. G.: Trophic structure on the West  
1008 Antarctic Peninsula shelf: Detritivory and benthic inertia revealed by  $\delta^{13}\text{C}$  and  $\delta^{15}\text{N}$  analysis, *Deep.*  
1009 *Res. Part II Top. Stud. Oceanogr.*, 55, 2502–2514, <https://doi.org/10.1016/j.dsr2.2008.06.009>, 2008.

1010 Montoya, J. P.: Natural abundance of  $^{15}\text{N}$  in marine planktonic ecosystems, in: *Stable Isotopes in*  
1011 *Ecology and Environmental Science: Second Edition*, edited by: Michener, R. and Lajtha, K., Blackwell  
1012 Publishing, 1–566, <https://doi.org/10.1002/9780470691854>, 2007.

1013 Moore, J. K., Abbott, M. R., and Richman, J. G.: Location and dynamics of the Antarctic Polar Front

- 1014 from satellite sea surface temperature data, *J. Geophys. Res. Ocean.*, 104, 3059–3073,  
1015 <https://doi.org/10.1029/1998JC900032>, 1999.
- 1016 Ng, H. C., Cassarino, L., Pickering, R. A., Woodward, E. M. S., Hammond, S. J., and Hendry, K. R.:  
1017 Sediment efflux of silicon on the Greenland margin and implications for the marine silicon cycle,  
1018 *Earth Planet. Sci. Lett.*, 529, 115877, <https://doi.org/10.1016/j.epsl.2019.115877>, 2020.
- 1019 Nielsdóttir, M. C., Bibby, T. S., Moore, C. M., Hinz, D. J., Sanders, R., Whitehouse, M., Korb, R., and  
1020 Achterberg, E. P.: Seasonal and spatial dynamics of iron availability in the Scotia Sea, *Mar. Chem.*,  
1021 130–131, 62–72, <https://doi.org/10.1016/j.marchem.2011.12.004>, 2012.
- 1022 Opfergelt, S. and Delmelle, P.: Silicon isotopes and continental weathering processes: Assessing  
1023 controls on Si transfer to the ocean, *Comptes Rendus - Geosci.*, 344, 723–738,  
1024 <https://doi.org/10.1016/j.crte.2012.09.006>, 2012.
- 1025 Orsi, H., Whitworth III, T., and Nowlin Jr, W. D.: On the meridional extent and fronts of the Antarctic  
1026 Circumpolar Current, *Deep Sea Res. Part I Oceanogr. Res. Pap.*, 42, 641–673,  
1027 [https://doi.org/10.1016/0967-0637\(95\)00021-W](https://doi.org/10.1016/0967-0637(95)00021-W), 1995.
- 1028 Passow, U. and De La Rocha, C. L.: Accumulation of mineral ballast on organic aggregates, *Global*  
1029 *Biogeochem. Cycles*, 20, 1–7, <https://doi.org/10.1029/2005GB002579>, 2006.
- 1030 Pauli, N.-C., Flintrop, C. M., Konrad, C., Pakhomov, E. A., Swoboda, S., Koch, F., Wang, X.-L., Zhang, J.-  
1031 C., Brierley, A. S., Bernasconi, M., Meyer, B., and Iversen, M. H.: Krill and salp faecal pellets  
1032 contribute equally to the carbon flux at the Antarctic Peninsula, *Nat. Commun.*, 12, 7168,  
1033 <https://doi.org/10.1038/s41467-021-27436-9>, 2021.
- 1034 Ploug, H., Iversen, M. H., and Fischer, G.: Ballast, sinking velocity, and apparent diffusivity within  
1035 marine snow and zooplankton fecal pellets: Implications for substrate turnover by attached bacteria,  
1036 *Limnol. Oceanogr.*, 53, 1878–1886, 2008.
- 1037 Popp, B. N., Laws, E. A., Bidigare, R. R., Dore, J. E., Hanson, K. L., and Wakeham, S. G.: Effect of  
1038 phytoplankton cell geometry on carbon isotopic fractionation, *Geochim. Cosmochim. Acta*, 62, 69–  
1039 77, [https://doi.org/10.1016/S0016-7037\(97\)00333-5](https://doi.org/10.1016/S0016-7037(97)00333-5), 1998.
- 1040 Popp, B. N., Trull, T., Kenig, F., Wakeham, S. G., Rust, T. M., Tilbrook, B., Griffiths, F. B., Wright, S. W.,  
1041 Marchant, H. J., Bidigare, R. R., and Laws, E. A.: Controls on the carbon isotopic composition of  
1042 Southern Ocean phytoplankton, *Global Biogeochem. Cycles*, 13, 827–843,  
1043 <https://doi.org/10.1029/1999GB900041>, 1999.
- 1044 Priddle, J. and Fryxell, G.: Handbook of the common plankton diatoms of the Southern Ocean:  
1045 Centrales except the genus *Thalassiosira*, British Antarctic Survey, Cambridge, UK, 159 pp., 1985.
- 1046 Rau, G. H., Froelich, P. N., Takahashi, T., and J., D. M. D.: Does sedimentary organic  $\delta^{13}\text{C}$  record  
1047 variations in quaternary ocean  $[\text{CO}_2(\text{aq})]$ , *Paleoceanography*, 6, 335–347, 1991.
- 1048 Raven, J. A.: Inorganic Carbon Acquisition by Marine Autotrophs, *Adv. Bot. Res.*, 27, 85–209,  
1049 [https://doi.org/10.1016/S0065-2296\(08\)60281-5](https://doi.org/10.1016/S0065-2296(08)60281-5), 1997.
- 1050 Rembauville, M., Blain, S., Armand, L., Quéguiner, B., and Salter, I.: Export fluxes in a naturally iron-  
1051 fertilized area of the Southern Ocean – Part 2: Importance of diatom resting spores and faecal  
1052 pellets for export, *Biogeosciences*, 12, 3171–3195, <https://doi.org/10.5194/bg-12-3171-2015>, 2015.
- 1053 Rembauville, M., Manno, C., Tarling, G. A., Blain, S., and Salter, I.: Strong contribution of diatom  
1054 resting spores to deep-sea carbon transfer in naturally iron-fertilized waters downstream of South  
1055 Georgia, *Deep. Res. Part I*, 115, 22–35, <https://doi.org/10.1016/j.dsr.2016.05.002>, 2016.
- 1056 Reynolds, B. C., Aggarwal, J., André, L., Baxter, D., Beucher, C., Brzezinski, M. A., Engström, E., Georg,

- 1057 R. B., Land, M., Leng, M. J., Opfergelt, S., Rodushkin, I., Sloane, H. J., Van Den Boorn, S. H. J. M.,  
 1058 Vroon, P. Z., and Cardinal, D.: An inter-laboratory comparison of Si isotope reference materials, *J.*  
 1059 *Anal. At. Spectrom.*, 22, 561–568, <https://doi.org/10.1039/b616755a>, 2007.
- 1060 Roberts, K., Granum, E., Leegood, R. C., and Raven, J. A.: Carbon acquisition by diatoms, *Photosynth.*  
 1061 *Res.*, 93, 79–88, <https://doi.org/10.1007/s11120-007-9172-2>, 2007.
- 1062 Roca-Marti, M., Puigcorbé, V., Iversen, M. H., Rutgers van der Loeff, M., Klaas, C., Cheah, W.,  
 1063 Bracher, A., and Masqué, P.: High particulate organic carbon export during the decline of a vast  
 1064 diatom bloom in the Atlantic sector of the Southern Ocean, *Deep Sea Res. Part II Top. Stud.*  
 1065 *Oceanogr.*, 138, 102–115, <https://doi.org/10.1016/j.dsr2.2015.12.007>, 2017.
- 1066 Salter, I., Kemp, A. E. S. S., Moore, C. M., Lampitt, R. S., Wolff, G. A., and Holtvoeth, J.: Diatom resting  
 1067 spore ecology drives enhanced carbon export from a naturally iron-fertilized bloom in the Southern  
 1068 Ocean, *Global Biogeochem. Cycles*, 26, 1–17, <https://doi.org/10.1029/2010GB003977>, 2012.
- 1069 Sathyendranath, S., Brewin, R., Brockmann, C., Brotas, V., Calton, B., Chuprin, A., Cipollini, P., Couto,  
 1070 A., Dingle, J., Doerffer, R., Donlon, C., Dowell, M., Farman, A., Grant, M., Groom, S., Horseman, A.,  
 1071 Jackson, T., Krasemann, H., Lavender, S., Martinez-Vicente, V., Mazeran, C., Mélin, F., Moore, T.,  
 1072 Müller, D., Regner, P., Roy, S., Steele, C., Steinmetz, F., Swinton, J., Taberner, M., Thompson, A.,  
 1073 Valente, A., Zühlke, M., Brando, V., Feng, H., Feldman, G., Franz, B., Frouin, R., Gould, R., Hooker, S.,  
 1074 Kahru, M., Kratzer, S., Mitchell, B., Muller-Karger, F., Sosik, H., Voss, K., Werdell, J., and Platt, T.: An  
 1075 Ocean-Colour Time Series for Use in Climate Studies: The Experience of the Ocean-Colour Climate  
 1076 Change Initiative (OC-CCI), *Sensors*, 19, 4285, <https://doi.org/10.3390/s19194285>, 2019.
- 1077 Sathyendranath, S., Jackson, T., Brockmann, C., Brotas, V., Calton, B., Chuprin, A., Clements, O.,  
 1078 Cipollini, P., Danne, O., Dingle, J., Donlon, C., Grant, M., Groom, S., Krasemann, H., Lavender, S.,  
 1079 Mazeran, C., Mélin, F., Müller, D., Steinmetz, F., Valente, A., Zühlke, M., Feldman, G., Franz, B.,  
 1080 Frouin, R., Werdell, J., and Platt, T.: ESA Ocean Colour Climate Change Initiative (Ocean\_Colour\_cci):  
 1081 Version 5.0 Data, NERC EDS Cent. Environ. Data Anal.,  
 1082 <https://doi.org/10.5285/1dbe7a109c0244aaad713e078fd3059a>, 2021.
- 1083 Schmidt, K., Atkinson, A., Stübing, D., McClelland, J. W., Montoya, J. P., and Voss, M.: Trophic  
 1084 relationships among Southern Ocean copepods and krill: Some uses and limitations of a stable  
 1085 isotope approach, *Limnol. Oceanogr.*, 48, 277–289, <https://doi.org/10.4319/lo.2003.48.1.0277>,  
 1086 2003.
- 1087 Scott, F. J. and Marchant, H. J. (Eds.): *Antarctic Marine Protists*, Australian Biological Resources  
 1088 Study, Canberra, 2005.
- 1089 Shen, C., Dupont, C. L., and Hopkinson, B. M.: The diversity of CO<sub>2</sub>-concentrating mechanisms in  
 1090 marine diatoms as inferred from their genetic content, *J. Exp. Bot.*, 68, 3937–3948,  
 1091 <https://doi.org/10.1093/jxb/erx163>, 2017.
- 1092 Sigman, D. M. and Fripiat, F.: Nitrogen isotopes in the ocean, *Encycl. Ocean Sci.*, 263–278,  
 1093 <https://doi.org/10.1016/B978-0-12-409548-9.11605-7>, 2019.
- 1094 Smetacek, V., Assmy, P., and Henjes, J.: The role of grazing in structuring Southern Ocean pelagic  
 1095 ecosystems and biogeochemical cycles, *Antarct. Sci.*, 16, 541–558,  
 1096 <https://doi.org/10.1017/S0954102004002317>, 2004.
- 1097 Strickland, J. and Parsons, T.: *A Practical Handbook of Seawater Analysis*, Fisheries Research Board of  
 1098 Canada, 405 pp., <https://doi.org/10.2307/1979241>, 1972.
- 1099 Sutton, J. N., Varela, D. E., Brzezinski, M. A., and Beucher, C. P.: Species-dependent silicon isotope  
 1100 fractionation by marine diatoms, *Geochim. Cosmochim. Acta*, 104, 300–309,

1101 <https://doi.org/10.1016/j.gca.2012.10.057>, 2013.

1102 Tamelander, T., Søreide, J. E., Hop, H., and Carroll, M. L.: Fractionation of stable isotopes in the Arctic  
1103 marine copepod *Calanus glacialis*: Effects on the isotopic composition of marine particulate organic  
1104 matter, *J. Exp. Mar. Bio. Ecol.*, 333, 231–240, <https://doi.org/10.1016/j.jembe.2006.01.001>, 2006.

1105 Thorpe, S. E., Heywood, K. J., Brandon, M. A., and Stevens, D. P.: Variability of the southern Antarctic  
1106 Circumpolar Current front north of South Georgia, *J. Mar. Syst.*, 37, 87–105,  
1107 [https://doi.org/10.1016/S0924-7963\(02\)00197-5](https://doi.org/10.1016/S0924-7963(02)00197-5), 2002.

1108 Torres Valdés, S., Painter, S. C., Martin, A. P., Sanders, R., and Felden, J.: Data compilation of fluxes  
1109 of sedimenting material from sediment traps in the Atlantic ocean, *Earth Syst. Sci. Data*, 6, 123–145,  
1110 <https://doi.org/10.5194/essd-6-123-2014>, 2014.

1111 Trimborn, S., Wolf-Gladrow, D., Richter, K. U., and Rost, B.: The effect of pCO<sub>2</sub> on carbon acquisition  
1112 and intracellular assimilation in four marine diatoms, *J. Exp. Mar. Bio. Ecol.*, 376, 26–36,  
1113 <https://doi.org/10.1016/j.jembe.2009.05.017>, 2009.

1114 Trull, T. W. and Armand, L.: Insights into Southern Ocean carbon export from the  $\delta^{13}C$  of particles  
1115 and dissolved inorganic carbon during the SOIREE iron release experiment, *Deep. Res. Part II Top.*  
1116 *Stud. Oceanogr.*, 48, 2655–2680, [https://doi.org/10.1016/S0967-0645\(01\)00013-3](https://doi.org/10.1016/S0967-0645(01)00013-3), 2001.

1117 Tuerena, R. E., Ganeshram, R. S., Humphreys, M. P., Browning, T. J., Bouman, H., and Piotrowski, A.  
1118 P.: Isotopic fractionation of carbon during uptake by phytoplankton across the South Atlantic  
1119 subtropical convergence, *Biogeosciences*, 16, 3621–3635, <https://doi.org/10.5194/bg-16-3621-2019>,  
1120 2019.

1121 Volk, T. and Hoffert, M. I.: Ocean Carbon Pumps: Analysis of relative strengths and efficiencies in  
1122 ocean driven atmospheric CO<sub>2</sub> changes, in: *The carbon cycle and atmospheric CO<sub>2</sub>: Natural variations*  
1123 *Archean to Present*, edited by: Sundquist, E. T. and Broecker, W. S., American Geophysical Union,  
1124 Washington, DC, 99–110, 1985.

1125 Wada, E. and Hattori, A.: Nitrogen isotope effects in the assimilation of inorganic nitrogenous  
1126 compounds by marine diatoms, *Geomicrobiol. J.*, 1, 85–101,  
1127 <https://doi.org/10.1080/01490457809377725>, 1978.

1128 Wada, E., Terazaki, M., Kabaya, Y., and Nemoto, T.: <sup>15</sup>N and <sup>13</sup>C abundances in the Antarctic Ocean  
1129 with emphasis on the biogeochemical structure of the food web, *Deep Sea Res. Part A, Oceanogr.*  
1130 *Res. Pap.*, 34, 829–841, [https://doi.org/10.1016/0198-0149\(87\)90039-2](https://doi.org/10.1016/0198-0149(87)90039-2), 1987.

1131 Ward, J. P. J., Hendry, K. R., Arndt, S., Faust, J. C., Freitas, F. S., Henley, S. F., Krause, J. W., März, C.,  
1132 Ng, H. C., Pickering, R. A., and Tessin, A. C.: Stable silicon isotopes uncover a mineralogical control on  
1133 the benthic silicon cycle in the Arctic Barents Sea, *Geochim. Cosmochim. Acta*, 329, 206–230,  
1134 <https://doi.org/10.1016/j.gca.2022.05.005>, 2022.

1135 Weir, I., Fawcett, S., Smith, S., Walker, D., Bornman, T., and Fietz, S.: Winter biogenic silica and  
1136 diatom distributions in the Indian sector of the Southern Ocean, *Deep. Res. Part I Oceanogr. Res.*  
1137 *Pap.*, 166, 103421, <https://doi.org/10.1016/j.dsr.2020.103421>, 2020.

1138 Wetzel, F., de Souza, G. F., and Reynolds, B. C.: What controls silicon isotope fractionation during  
1139 dissolution of diatom opal?, *Geochim. Cosmochim. Acta*, 131, 128–137,  
1140 <https://doi.org/10.1016/j.gca.2014.01.028>, 2014.

1141 White, W. M., Albarède, F., and Télouk, P.: High-precision analysis of Pb isotope ratios by multi-  
1142 collector ICP-MS, *Chem. Geol.*, 167, 257–270, [https://doi.org/10.1016/S0009-2541\(99\)00182-5](https://doi.org/10.1016/S0009-2541(99)00182-5),  
1143 2000.

- 1144 Whitehouse, M. J., Priddle, J., Trathan, P. N., and Brandon, M. A.: Substantial open-ocean  
1145 phytoplankton blooms to the north of South Georgia, South Atlantic, during summer 1994, Mar.  
1146 Ecol. Prog. Ser., 140, 187–197, <https://doi.org/10.3354/meps140187>, 1996.
- 1147 Young, J. N., Heureux, A. M. C., Sharwood, R. E., Rickaby, R. E. M., Morel, F. M. M., and Whitney, S.  
1148 M.: Large variation in the Rubisco kinetics of diatoms reveals diversity among their carbon-  
1149 concentrating mechanisms, J. Exp. Bot., 67, 3445–3456, <https://doi.org/10.1093/jxb/erw163>, 2016.
- 1150